on the gel strength parameter, S, evaluated from the relationship¹⁶⁻¹⁹ G'(ω) = Γ (1-n)cos(n π /2)S ω ⁿ where Γ (1-n) is the Legendre Γ function. It is evident that the gel strength increases with increasing acid ratio and reaches its highest value acid ratio = 0.39, then decreases slightly. Thus, at low acid ratio, the critical gel cluster is relatively weak, at high acid ratio it is stronger.

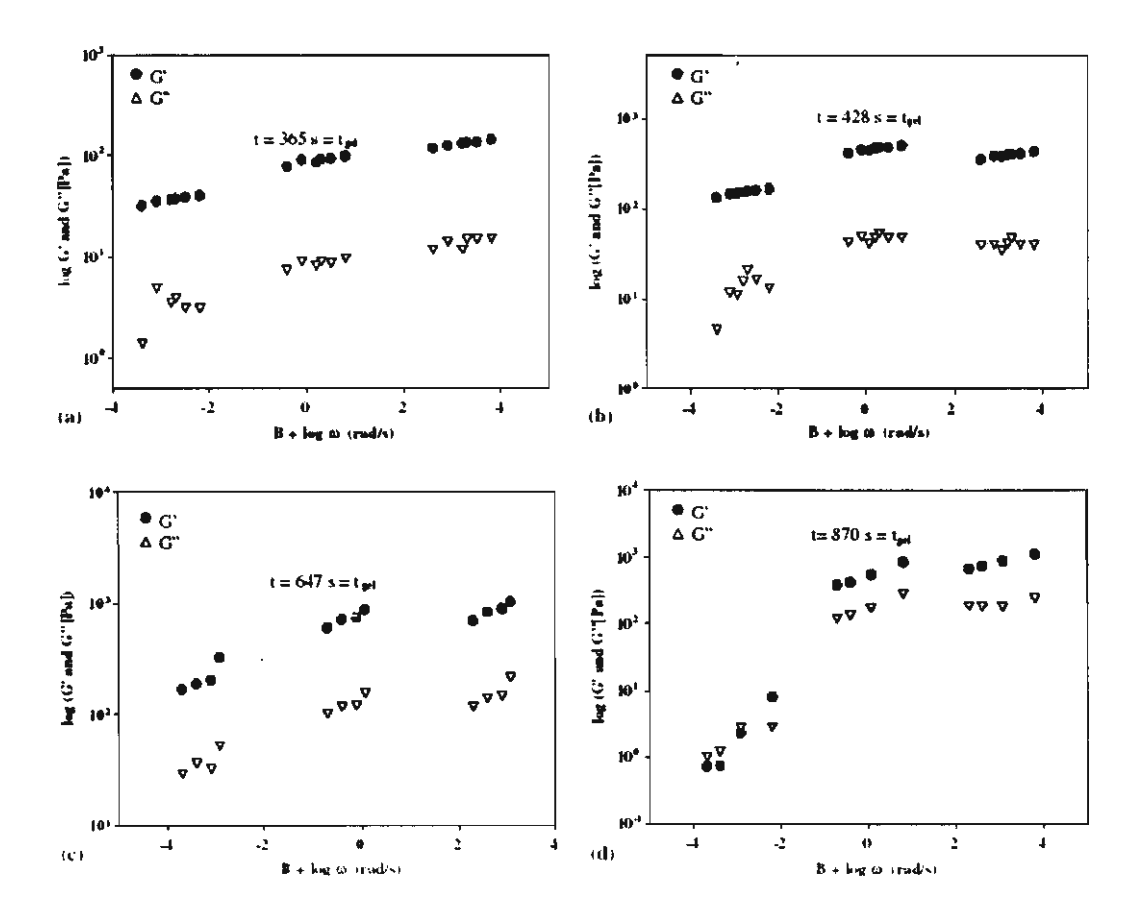
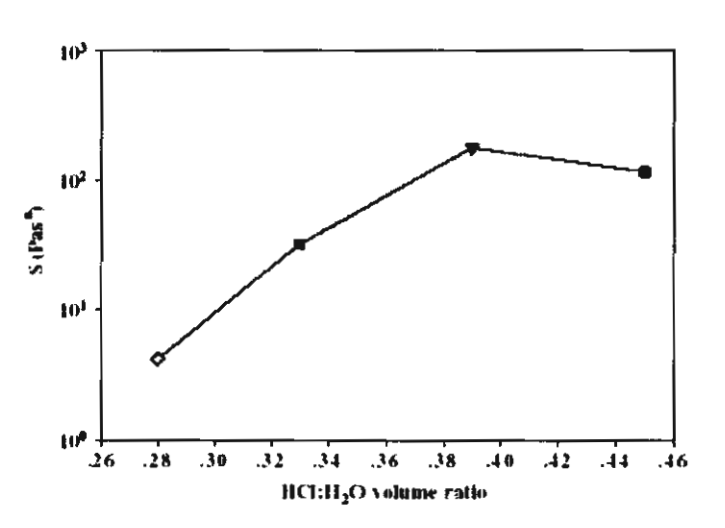


Figure 9 The frequency dependence curves of G' (ω) and G'' (ω) at (\bullet) pregel stage(B = -3),(\blacksquare) gel point,and (B = 0),and (\triangle) postgel stage (B = 3) of a.) 0.28, b.) 0.33, c.) 0.39 and d.) 0.45 HCl:H₂O ratios.

Figure 10 The plot of gel strength parameter S at the gel point as a function of HCl:H₂O volume ratio: 0.28 (♠), 0.33 (■), 0.39(♠) and 0.45 (♠).



According to the model of Muthukumar²⁰ the fractal dimension of the critical gel cluster can be obtained from the viscoelastic exponent n as $n = d(d+2-2d_f)/2(d+2-d_f)$ where d = spatial dimension = 3. The effect of acid ratio on the fractal dimension of incipient gel is shown in fig. 11 and table 2. The fractal dimension decreases with increasing the acid ratio. A lower fractal dimension mean that the molecular weight grows slower with radius, i.e. $M \sim R^{d_f}$. Thus the critical gel at high acid ratio has a more open structure than at low acid ratio. This is somewhat surprising since we expect the cross-link density to be higher at higher acid ratio. Again we attribute this result to the heterogeneous character of the system at the gel point. The particles which comprise the gel network at low acid ratio are less hydrated and hence more dense than those at higher acid ratio.

Figure 11 The plot of fractal dimension of the critical gel coluster as a function of acid ratio

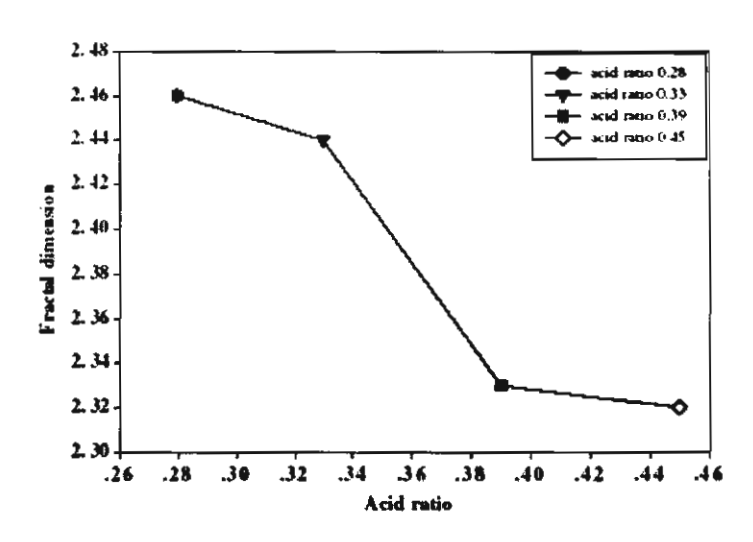


Table 2 Summary of viscoelastic exponent, fractal dimension, and gelation time(s) at various HCl:H₂O volume ratios.

Acid ratio	n	df	Gelation time (s)
0.28	0.05	2.46	365
0.33	0.07	2.44	428
0.39	0.19	2.33	647
0.45	0.20	2.32	870

Figure 1? shows the frequency dependence of the dynamic viscosity at pregel stage, gel point, and postgel stage. Consistent with the highly elastic behavior evident in figure 9, at all stages $\eta^*(\omega)$ exhibits power law frequency dependence with an exponent at the gel point of n-1. The time dependence of the complex viscosity at low frequency $(\omega=0.4 \text{ rad/s})$ is illustrated in fig. 13. The location of the gel point for each system as determined by the Winter criteria 16-19 are indicated by arrows. At low acid ratio, the viscosity is initially high but approaches an asymptotic value which is relatively low. At high acid ratio, the viscosity is initially low but reaches a high asymptotic value. Thus, the gel strength and asymptotic complex viscosity are self-consistent and indicate that the gel becomes stronger under high acidity conditions. We interpret these results as indicating that at low acid, the precursor particles are poorly hydrated and form a more heterogeneous weak gel structure. At high acid, the particles are well solvated and form a less heterogeneous (more open) yet stronger network.

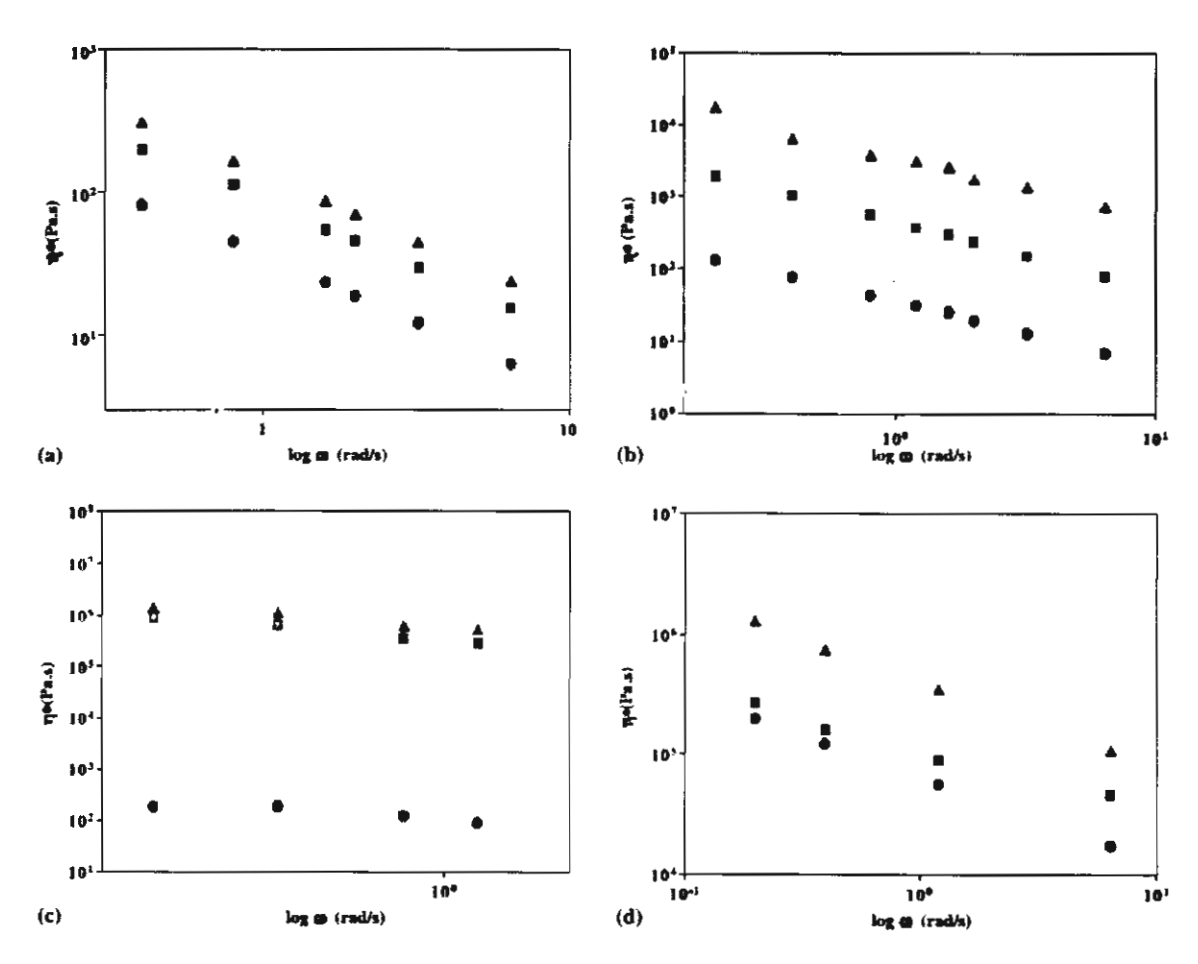


Figure 12 The effect of frequency on the complex viscosity at pregel stage, gel point, and postgel stage of a.) 0.28, b.) 0.33, c.) 0.39 and d.) 0.45 HCl:H₂O volume ratios

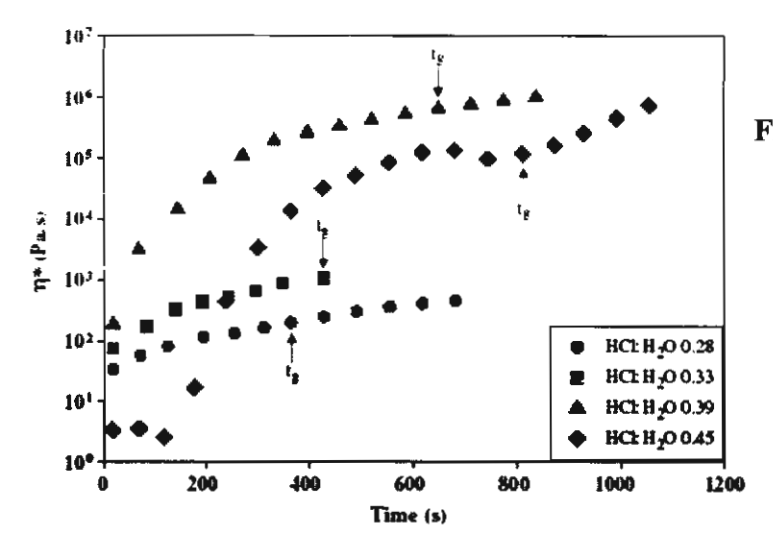


Figure 13 The time evolution of the complex viscosity (at fixed frequency of 0.4 rad/s) of a) 0.28, b) 0.33, c) 0.39 and d) 0.45 HCl:H₂O volume ratio

Conclusions

Anatase TiO₂ nanoparticles were successfully prepared by sol-gel technology, using inexpensive and moisture-stable titanium glycolate as precursor in 1M HCl solution. The calcination temperature and the HCl:H₂O volume ratio has a substantial influence on the surface area, phase transformation, and morphology of the products. Anatase titania is produced at calcination temperatures in the range 600° to 800°C, above which transformation to rutile occurs. Increase of temperature results in anatase of higher crystallinity but lower specific surface area, and induces a morphological change from large irregular agglomerates to more homogeneous particles of spherical shape. From XRD measurements of average grain sizes, we deduce that nucleation rate dominates the kinetics at low temperatures, and growth rate becomes the controlling factor at high temperature and low HCl:H2O ratios. Increase of HCl:H2O ratio results in a small but significant decrease in porosity. The highest specific surface area 125 m²/g is obtained at lowest HCl:H₂O ratio 0.28 and lowest calcination temperature (600°C). From rheological analysis, as evaluated by the Winter criteria, the gelation time increases with increase of HCl:H2O volume ratio. The fractal dimension determined from the frequency scaling exponent of the modulus at the gel point indicates a denses critical gel structure at low acid ratio. However the complex viscosity and gel strength increase as a function of acid ratio. We interpret this behavior as indicative that, at low acidity, the gel is composed of poorly hydrated particles forming a dense but weak structure. Increased acidity increases hydration and cross-link density leading to a more open and stronger gel network.

References

- 1. J. Yang, S. Mei, J.M. Ferriera, Mat. Sci. Eng. C-Biomim 15 (2001) 183.
- 2. H. kominami, M. kohno, Y. Takada, M. Inoue, T. Inui, Y. Kera, Ind. Eng. Chem. Res. 38 (1999) 3931.
- K.M.S. Khalil, T. Baird, M.I. Zaki, A.A. El-Samahy, A.M. Awad, Colloid Surface A 132 (1998) 31.
- 4. K.M.S. Khalil, M.I. Zaki, Powder Technol. 120 (2001) 256.
- 5. Y. Zhang, A. Weidenkaff, A. Reller, Mater. Lett. 54 (2002) 375.
- 6. Y. Wei, R. Wu, Y. Zhang, Mater. Lett. 41 (1999) 101.
- 7. Y. Sun, A. Li, M. Qi, L. Zhang, X. Yao, Mat. Sci. Eng. B86 (2001) 185.

- 8. E.J. Kim, S.H. Hahn, Mater. Lett. 49 (2001) 244.
- M. Wu, G. Lin, D. Chen, G. Wang, D. He, S. Feng, R. Xu, Chem. Mater. 14 (2002) 1974.
- 10. Kao, S.N. Bhattacharya, J. Rheol. 42 (1998) 493.
- 11.N. Phonthammachai, T. Chairassameewong, E. Gulari, A.M. Jamieson, S. Wongkasemjit, J. Met. Mat. Min. 12 (2002) 23.
- 12. Q. Zhang, L. Gao, J. Gac, Appl. Catal. B-Solid 26 (2000) 207.
- 13. Y. Zhang, A. Weidenkaff, A. Reller, Mater. Lett. 54 (2002) 375.
- 14. J. Zhao, Z. Wang, L. Wang, H. Yang, M. Zhao, Mater. Chem. Phys. 63 (2000) 9.
- 15. H.H. Winter, F. Chambon, J. Rheol. 30 (1986) 367.
- 16. A.L. Kjoniksen, B. Nystrom, Macromolecules 29 (1996) 5215.
- 17. M. Jokinen, E. Gyorvary, J.B. Rosenholm, Colloid Surface A 141 (1998) 205.
- 18. B. Nystrom, A.L. Kjonoksen, B. Lindman, Langmuir 12 (1996) 3233.
- W. Charoenpanijkarn, M. Suwankruhasn, B. Kesapabutr, S. Wongkasemjit,
 A.M. Jamieson, Eur. Ploym. J 37 (2001) 1441.
- 20. Muthukumar, M, Macromocules 22 (1989) 4656.

CHAPTER VI

STRUCTURAL AND CRYSTALLIZATION OF HIGH Ti LOADED TS-1 ZEOLITE

Abstract

The TS-1 with high Ti loading was successfully synthesized using low cost and moisture-stable precursors, titanium glycolate and silatrane. The microwave instrument was used as a heating source for synthesis. The effects of the compositions (TPA⁺, NaOH, H₂O) and conditions (aging time, reaction temperature, reaction time) were studied. The Si:Ti molar ratios were varied from 100.00-5.00 and the ability of Ti incorporated into the zeolite framework was studied. The XRD, FT-IR, SEM and DR-UV were used to characterize the TS-1 samples and all samples showed the characteristic of MFI type. The small amount of extra-framework titanium dioxide was also identified at 5.0 Si:Ti molar ratio. The photocatalytic decomposition of 4-NP was used to test the activity of TS-1 samples and the results of all samples showed high efficiency in photocatalytic decomposition (PCD).

Introduction

Titanium silicate-1 (TS-1), a Ti-containing zeolite with the MFI structure, is a highly selective and active crystalline microporous heterogeneous oxidation catalyst employing H₂O₂ under mild conditions. The titanium in TS-1 isomorphously replaces silicon in a tetrahedral site of the MFI silicate lattice. It combines the advantages of the high coordination ability of Ti⁴⁺ ions with the hydrophobicity of the siliate framework, while retaining the spatial selectivity and specific local geometry of the active sites of the molecular sieve structure¹. The catalytic properties of titanosilicate are unique with a variety of liquid-phase oxidation, such as phenol hydroxylation, olefin epoxidation, cyclohexanone ammoximation and the oxidation of saturated hydrocarbons and alcohol²⁻³. With H₂O₂, solvolysis produces TiOOH and SiOH with the former giving rise to the active catalytic oxidation center.

After year 1983 which Taramasso et al ⁴ reported the hydrothermal synthesis of TS-1 for the first time, there are many researches tried to increase the amount of Ti^{IV} in the zeolite framework. A major problem often encountered the synthesis of TS-1 molecular sieve is the precipitation of oxide of the titanium outside the lattice framework, leading to samples, inactivity for oxidation reactions⁵. The synthesis of materials containing isolated tetrahedral Ti is rather difficult, given its strong tendency to polymerize in aqueous systems which often resulting in the formation of separate titanium dioxide phase¹. Two methods to synthesize were described in the original patent using different Si sources, tetraethylorthosilicate (TEOS) and Ludox colloidal silica. TS-1 is usually synthesized using tetrapropylammonium hydroxide (TPAOH) solution, which acts as the structure directing agent and provides the alkalinity necessary for the crystallization of the zeolite⁶. From many previous works, maximum amount of Ti^{IV} that can incorporated in the zeolite framework is at Si:Ti less than 35^{1,3,6}.

Microwave-assisted-hydrothermal synthesis is the process has been used for the rapid synthesis of numerous ceramic oxides and porous materials. It offers many advantages over conventional synthesis, including the increase of temperature of the reactant to a desired range quickly in a few minutes, homogeneous nucleation, fast supersaturation by the rapid dissolution of precipitated gels and shorter crystallization time. The heat is supposedly induced by the friction of molecular rotation enhanced by microwave irradiation, thus, it is possible to heat the reactants selectively and homogeneously from inside. Furthermore, It is energy efficient and economical⁷⁻⁸.

In this work, we synthesized the TS-1 zeolite from moisture stable and low cost starting materials, silatrane and titanium glycolate, used for silica and titanium dioxide sources, and TPABr as a template. The hydrothermal treatment by microwave heating and various amounts of Ti incorporated in the zeolite framework were studied. The samples were characterized using XRD, SEM, FT-IR and DR-UV. The photocatalytic decomposition of 4-NP was used to test the activity of TS-1 samples.

Experimental

Materials

Titanium dioxide (surface area 12 m²/g) was purchased from Sigma-Aldrich Chemical Co. Inc. (USA) and used as received. Ethylene glycol (EG) was purchased from Malinckrodt Baker, Inc. (USA) and purified by fractional distillation at 200°C under nitrogen atmosphere, before use. Triethylenetetramine (TETA) was purchased from Facai Polytech. Co. Ltd. (Bangkok, Thailand) and distilled under vacuum (0.1 mm/Hg) at 130°C prior to use. Acetonitrile was purchased from Lab-Scan Company Co. Ltd. and purified by distilling over calcium hydride powder. 4-Nitrophenol was purchased from Sigma-Aldrich Chemical Co. Inc. (USA).

Instrumental

Fourier transform infrared spectra (FT-IR) were recorded on a VECOR3.0 BRUKER spectrometer with a spectral resolution of 4 cm⁻¹ using transparent KBr pellets containing 0.001 g of sample mixed with 0.06 g of KBr. Thermal gravimetric analysis (TGA) was carried out using a Perkin Elmer thermal analysis system with a heating rate of 10°C/min over 30°-800°C temperature range.

Preparation of titanium glycolate

The procedure adopted followed previous work⁹. A mixture of TiO₂ (2g, 0.025 mol) and TETA (3.65g, 0.0074 mol) was stirred vigorously in excess EG (25 cm³) and heated to 200°C for 24 h. The resulting solution was centrifuged to separate the unreacted TiO₂. The excess EG and TETA were removed by vacuum distillation to obtain a crude precipitate. The white solid product was washed with acetonitrile, dried in a vacuum desiccator and characterized using FTIR and TGA.

FTIR: 2927-2855 cm⁻¹ (vC-H), 1080 cm⁻¹ (vC-O-Ti bond), and 619 cm⁻¹ (vTi-O bond). TGA: one sharp transition at 340°C with 46.95% ceramic yield corresponding to Ti(OCH₂CH₂O)₂.

Preparation of silatrane⁹

A mixture of Si(OH)₂ (6g, 0.1 mol) and TEA (18.648g, 0.125 mol) was stirred vigorously in excess EG (100 cm³) and heated to 200°C for 10 h. The resulting solution was vacuumed to remove EG to obtain a crude precipitate. The white solid product was washed with acetonitrile, dried in a vacuum desiccator and characterized using FTIR and TGA.

Fi-IR: 3422 cm-1 (ν O-H), 2986-2861 cm-1 (ν C-H), 2697 cm-1 (ν N-Si), 1459-1445 cm-1 (δ C-H), 1351 cm-1 (δ C-N), 1082 cm-1 (δ Si-O-C), 579 cm-1 (ν N-Si). TGA: one sharp transition at 380°C with 21.6% ceramic yield corresponding to N[CH₂CH₂O]₃SiOCH₂CH₂N(CH₂CH₂OH)₂.

Preparation of TS-1 zeolite

Hydrothermal syntheses were carried out using microwave irradiation. The TS-1 initial solution molar composition of gel SiO₂:0.1TiO₂:0.1TPA⁺:0.4NaOH:114H₂O. The effects of conditions were studied by varying the aging time (20, 60, 70, 90, 110, 130, 150, 170h), reaction time (5, 10, 15, 20h) and reaction temperature (120, 150, 180°C), amounts of TPA⁺, NaOH and H₂O. study of the Ti incorporated in the zeolite framework, $SiO_2:xTiO_2:0.3TPA^+:0.4NaOH:114H_2O$ (x = 0.1, 0.3, 0.5, 0.7, 1.0, 1.3, 1.7,2.0) was used. The solution was then aged at room temperature for 110h. After aging, the solution was transferred into Teflon vessel and heated under microwave irradiation at 150°C for various reaction times. The obtained TS-1 zeolite was washed several times with distilled water, dried at 60°C overnight and calcined at 550°C for 2h (0.5°C/min).

Photocatalytic decomposition of 4-nitrophenol

Photocatalytic reactions were carried out in a 250 ml batch reactor with a gas inlet and outlet at the flow rate of O₂ gas 20 ml/min. The cooling water jacket was used to control the temperature at 30°C. The suspensions were illuminated by using a Hg Philip UV lamp. The concentration of 4-NP was 40 ppm and the solution was continuous magnetically stirred. The TS-1 zeolite prepared at Si/Ti molar ratios of 100.00, 14.29, 7.69 and 5.00 was added in the solution with 0.8 g/l of catalyst, 10

mmol/l H₂O₂ was then slowly dropped. The samples were taken out and analyzed the concentration of 4-NP using Shimadzu UV-240 spectrophotometer.

TS-1 characterization

TS-1 samples were characterized by various techniques. XRD patterns were characterized using a D/MAX-2200H Rigaku diffractometer with CuKα radiation on specimens prepared by packing sample powder into a glass holder. The diffracted intensity was measured by step scanning in the 2θ range between 5° to 50°. Fourier transform infrared spectra (FT-IR) were recorded on a VECOR3.0 BRUKER spectrometer with a spectral resolution of 4 cm⁻¹ using transparent KBr pellets containing 0.001 g of sample mixed with 0.06 g of KBr. Samples were prepared for SEM analysis by attachment to aluminum stubs, after pyrolysis at 550°C. Prior to analysis, the specimens were dried in a vacuum oven at 70°C for 5 h followed by coating with gold via vapor deposition. Micrographs of the pyrolyzed sample surfaces were obtained at x7,500 magnification. Diffuse reflectance ultraviolet-visible (DR-UV) spectra were analyzed

Results and Discussion

Synthesis of TS-1

TS-1 is successfully synthesized by microwave hydrothermal treatment using silatrane and titanium glycolate as precursors in the condition with NaOH and TPABr. The XRD pattern (figure 1) shows the characteristic of MFI structure as reported by many literatures $^{1,3,10-11}$. The single peaks at $2\theta = 24.4^{\circ}$ indicate a change from monoclinic symmetry (silicate) to orthorhombic symmetry (TS-1) 1,12 . The FT-IR spectra of TS-1 in the framework Ti-O-Si bond stretching region shows an absorption band located at 960 cm^{-1} (figure 2). This band has been also observed in Ti-containing zeolites, being mainly assigned to the stretching mode of [SiO₄] tetrahedral bond with Ti atoms $^{13-14}$. However, such assignment has been interpreted in term of Si-OH groups with many defect structures 15 . The bands at 550 and 800 cm $^{-1}$ are assigned to δ (Si-O-Si) and υ (Si-O-Si), respectively. The diffuse reflectance spectra as figure 3 shows only one absorption band with a maximum at 210 nm, attribute to tetra-coordinated titanium, and there is no peak at 330 nm which is the peak of titanium dioxide extra-framework.

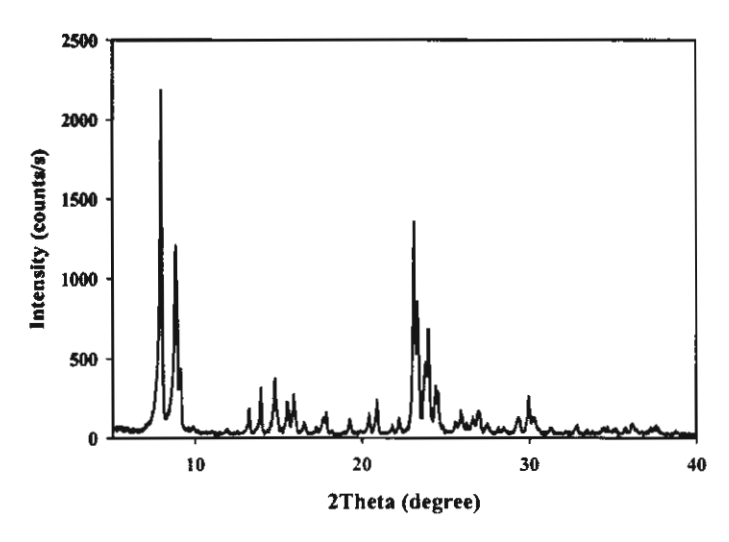


Figure 1 The XRD pattern of calcined TS-1 sample.

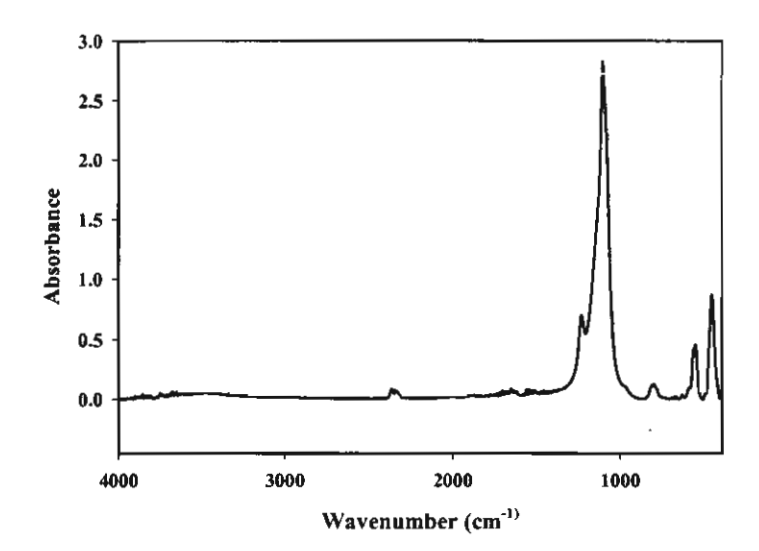


Figure 2 The FT-IR spectra of calcined TS-1 sample.

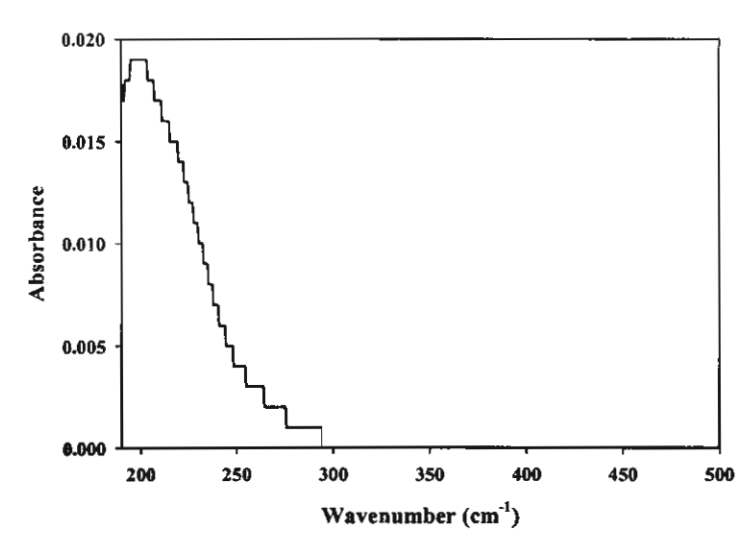


Figure 3 The DR-UV spectra of calcined TS-1 sample.

Effect of crystallization conditions and compositions of TS-1

1 Effect of reaction temperature

The effect of reaction temperature is studied by varying the temperature at 120°, 150° and 180°C. The synthesis formula is Si:0.1Ti:0.4NaOH: 0.1TPA:114H₂O. Figure 4 shows the XRD patterns of all samples, the intensity of peak increases as the reaction temperature. Its mean that when increasing the reaction temperature lead to the higher rate of crystallization. From the SEM micrograph of calcined samples, the crystal size increases with the reaction temperature. At 120°C (figure 5.1), the crystals have round shape and not uniform (0.5-2.5µm). As increasing the temperature to 150°C (figure 5.2), the crystals are uniform with cubic structure (1.µm). The largest crystal size (4µm) is observed at 180°C (figure 5.3) and indicates larger growth in c direction with hexagonal shape. When rising the temperature to 180°C, the degradation of the organic template is occurred. From the result, the suitable reaction temperature for a smallest and uniformly crystal is at 150°C.

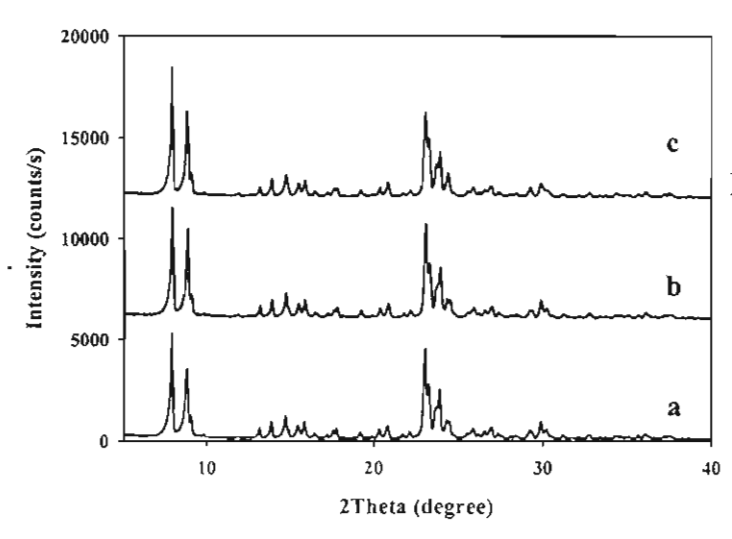


Figure 4 The XRD pattern of TS-1 samples at various reaction temperatures of a) 120°, b) 150° and c) 170°C.

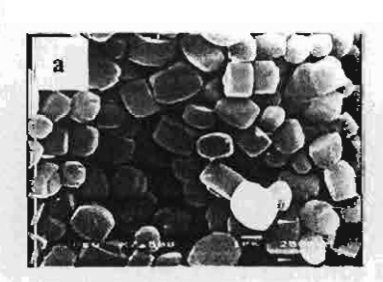






Figure 5. The SEM micrograph of TS-1 sample at various reaction temperatures of a) 120°, b) 150° and c) 170°C.

The Si:0.1Ti:0.4NaOH:0.1TPA:114H₂O formula is used to study the effect of reaction time to the crystallization of TS-1 zeolite. The reaction times are varies from 5, 10, 15 and 20 h at reaction temperature 150°C. The results show that at low reaction time the amorphous phase occurs and the conversion to TS-1 zeolite is lower than at higher time. It is mean that increasing the reaction time causes the increasing of the rate of crystallization. The SEM micrograph (figure 6) shows the large crystal size (5µm) at 5h and the size decreases dramatically to 1.3µm at 15h, the crystals have uniformly cubic shape. Increasing the reaction time to 20 h causes the larger crystal size and has a higher growth in b direction.

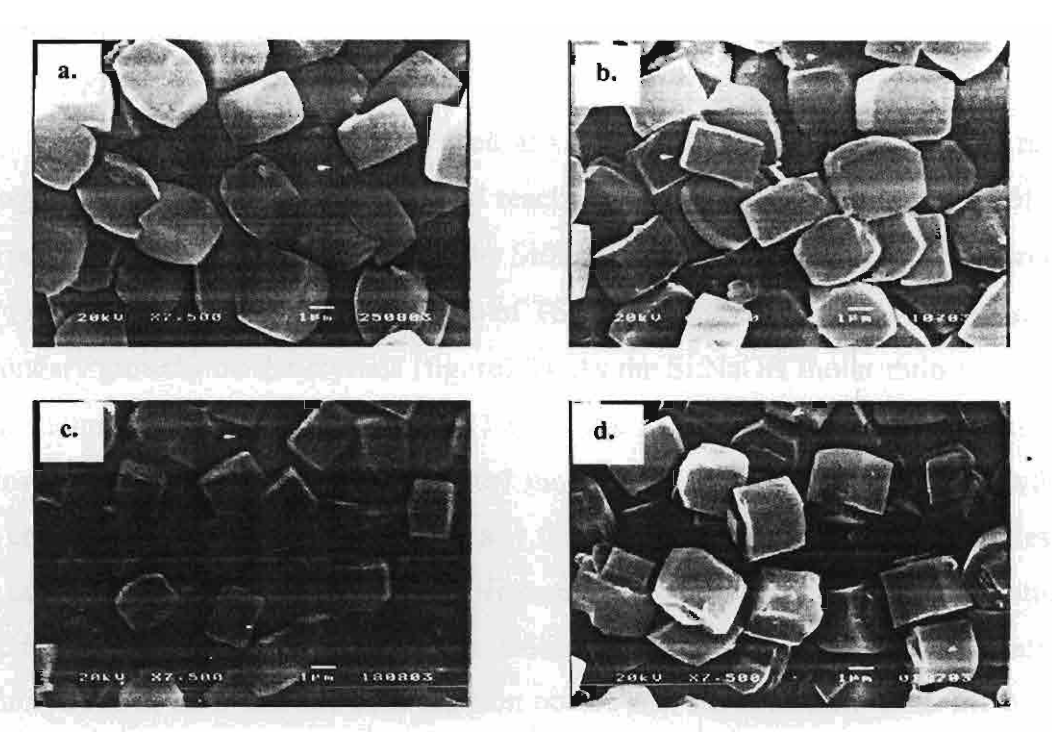


Figure 6. The SEM micrograph of TS-1 samples at various reaction times of a) 5, b) 10, c) 15 and d) 20h.

3 Effect of Aging time

The TS-1 samples at varies aging times (20, 60, 70, 90, 110, 130, 150 and 170h) are carried out at Si:0.1Ti:0.4NaOH:0.1TPA:114H₂O, reaction temperature 150°C and reaction time 15h. From the SEM micrographs in figure 7, at lower aging time, the large crystal sizes are formed with lower conversion to the TS-1 zeolite and present the large amount of amorphous phase. When the time increases, the crystal size becomes smaller until at aging time 130h the size increases again. The hydrolysis and condensation

reactions of silatrane and titanium precursors cause the polymerization to form the network and initially at low aging time the hydrolysis of precursor does not involve all the alkyl ligand, therefore, some organic ligands still present in the solution. The remaining organic ligand can participate with the organic template and form a primary unit, then the primary units are agglomerate and the nucleation occurs. At longer aging time, the large amount of primary particles occurs and results in the higher agglomeration and crystallization rate caused the smaller size with higher formation of zeolite after hydrothermal synthesis, which the growth rate is dominant. At longer aging time (130h), the limit of the primary unit formation occurs, therefore, the agglomeration occurs at the former nuclei.

4 Effect of NaOH:Si

The effect of NaOH:Si is studied at varying ratio from 0.1 to 1.0 mol ratio at aging time 110h, reaction time 15h and reaction temperature 150°C. At 0.1 mol ratio, the product is amorphous as shown in the SEM micrograph (figure 8). When increasing the ratio to 0.3, a very large crystal size of TS-1 zeolite is occurred (10µm) with many secondary growths on the crystals (figure 7.2). As the Si:NaOH molar ratio increases to 0.4, the uniform and smaller crystals (1.3 µm) are formed (figure 7.3). Increasing the ratios to 0.5 causes the larger size and 0.7 molar ratio has many secondary growths on the crystals (figures 7.4 and 7.5). Until at 1.0 molar ratio (figure 7.6), the particles loss the cubic shape. The increasing of NaOH causes the increasing in the concentration of reactive species available in solution for zeolite nucleation which NaOH accelerates the hydrolysis rate, after that the condensation occurs and starts to form a zeolite network with greater numbers of nuclei are generated and smaller particle size products are formed (0.3 molar ratio). At large amount of NaOH, the hydrolysis increases and the large crystals with secondary growths are formed (0.5 and 0.7 molar ratios). When increasing to a very high amount of NaOH, the sodium will efficiently occupy the surface of the silica gel particles cause the retardation of the nucleation because the TPA-Silica interaction is greatly reduced. A large part of the silica is in the core of the gel bodies and not accessible for nucleation formation 16.

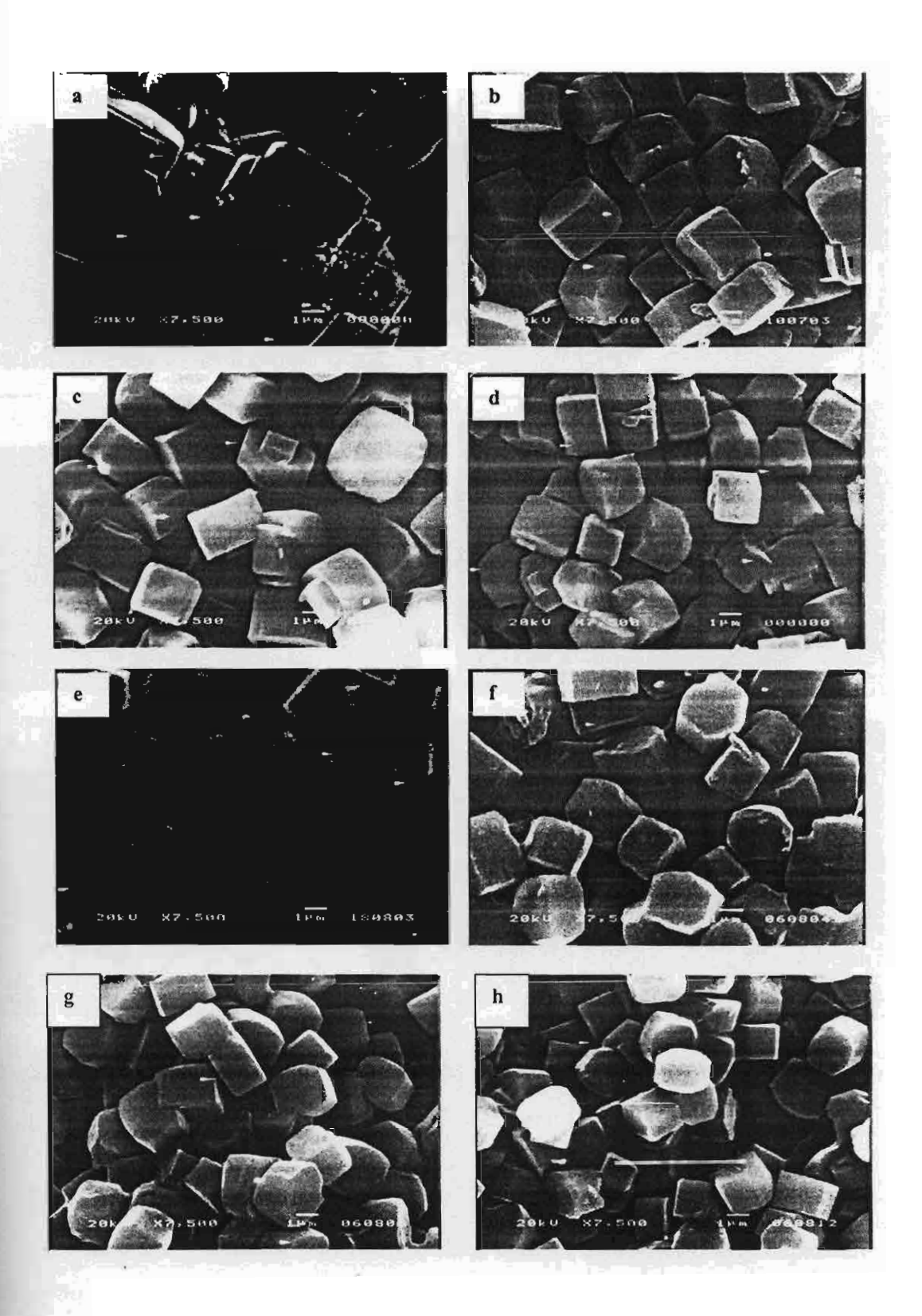


Figure 7. The SEM micrograph of TS-1 samples at various aging times of a) 20, b) 60, c) 70, d) 90, e) 110, f) 130, g) 150 and h) 170h.

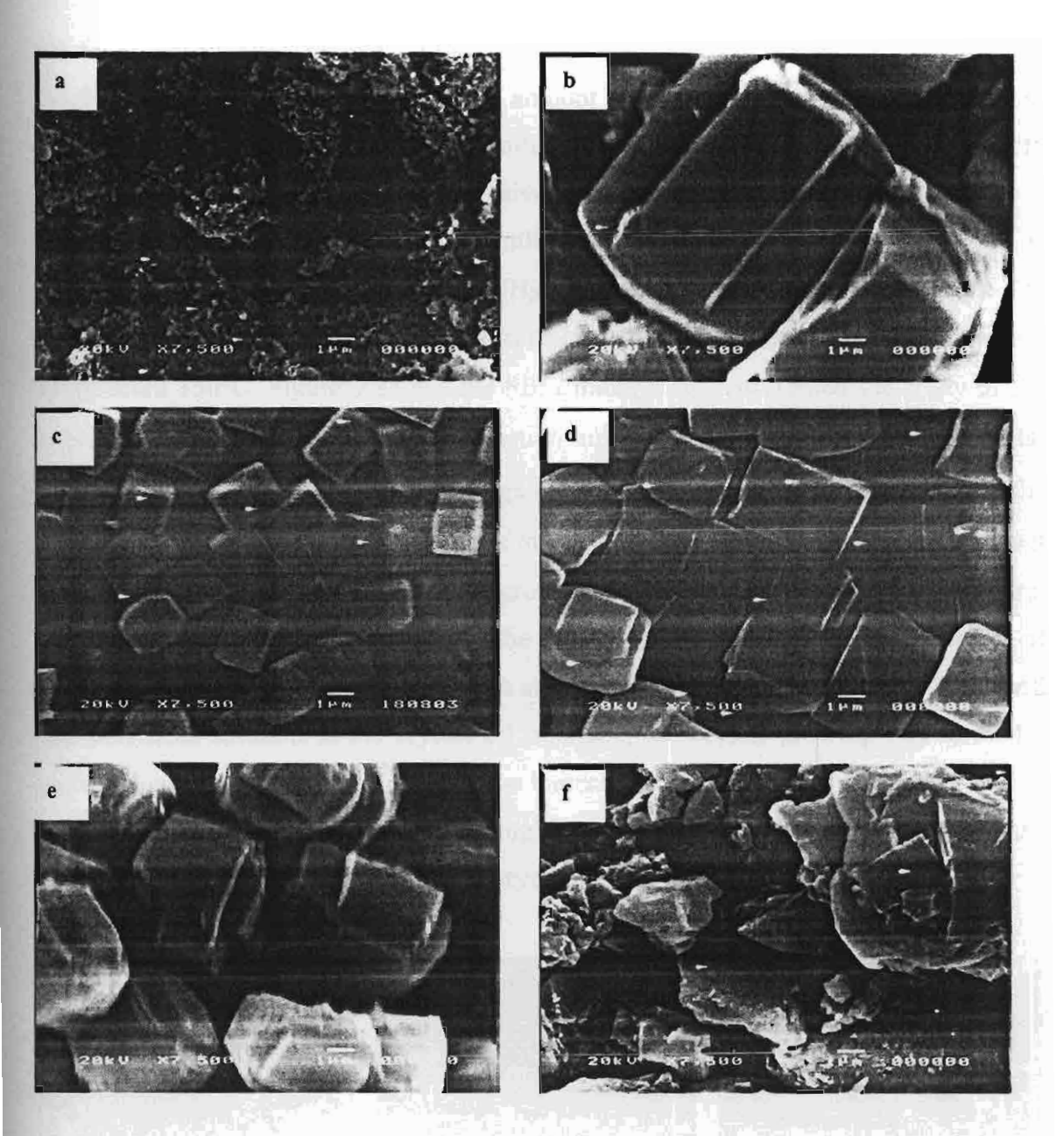


Figure 8. The SEM micrographs of TS-1 samples at various NaOH:Si molar ratios of a) 0.1, b) 0.3, c)0.4, d) 0.5, e) 0.7 and f) 1.0.

5 Effect of TPA:Si

The steric stabilization of nuclear-sized entities, is also critically dependent on the cation balance. The TPA⁺ cation is widely used in the synthesizing of zeolite, the bulky quaternary ammonium cations adsorbed on to particle surfaces provide steric stabilization, preventing aggregation upon collision¹⁶. There are many types of template use for synthesize the zeolite such as TPAOH, TBABr, 1,6-hexanediamine and TPABr. Wang et al.⁶ found that the synthesis by using TBABr will produce a favorable effect on

the formation of ZSM-11 and synthesize by 1,6-hexanediamine can use only for low titanium content which increasing the amount of titanium leads to a decrease of crystallinity. To decrease the cost of synthesis, TPAOH is replaced by TPABr. From many works TPABr showed a good selective oxidation reaction^{6,12}.

In our work, TPABr is used to synthesize TS-1 zeolite and the effect of TPA⁺ is studied at Si:0.1Ti:0.4NaOH: xTPA⁺:114H₂O (x = 0.05, 0.1, 0.2, 0.3, 0.4 and 0.5). The crystallization conditions are at aging time 110 h, reaction time 15h and reaction temperature 150°C. Figure 9 shows the SEM micrograph represented the study of the effect of TPA⁺:Si at aging time 110h, reaction time 15h, 150°C and 0.4 Si:NaOH molar ratio. At low molar ratio (3.05), the large crystals are formed (10μm). Increasing the amount of TPA⁺ causes the decreasing of the crystal size (1.2μm at 0.3 molar ratio) but at large amount of TPA⁺, the secondary growths occur (0.4 and 0.5 molar ratios). From the explanation of the Koegler *et al.*¹⁷, the nucleation starts to occur on the surface of the large gel sphere; both TPA⁺ and silica are abundance, into the gel sphere. TPA⁺ will transport from solution to the crystal/gel interface, the crystal growing and formed a perfected cubic shape. Its mean that if we increase the amount of TPA⁺, it will lead to the higher nucleation as shown here. At higher TPA⁺, the dendritic growth occurs at the surface of zeolite. This is indicative of very high supersaturation.

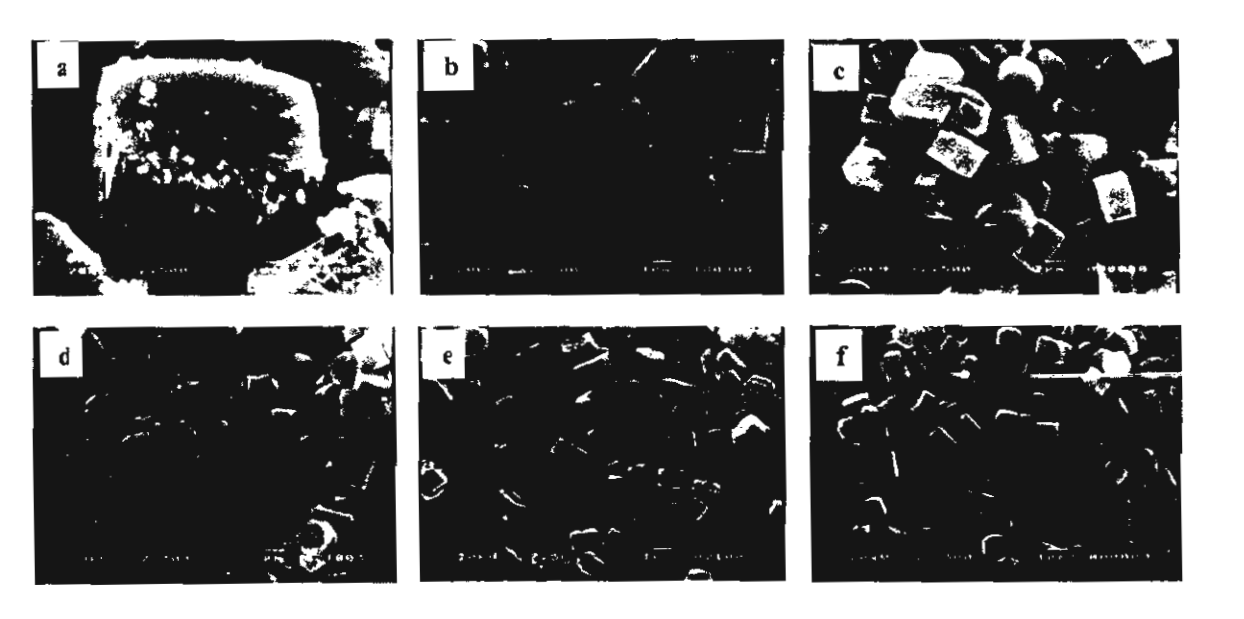


Figure 9. The SEM micrographs of TS-1 samples at various TPA:Si molar ratios of a) 0.05, b) 0.1, c) 0.2, d) 0.3, e) 0.4 and f) 0.5.

6 Effect of H₂O:Si ratio

The dilution is studied at Si:0.1Ti:0.4NaOH:0.3TPA:xH₂O (x = 80, 114, 140, 170 and 200). The reaction time is 15h, 150°C and aging time 110h. From the SEM micrograph as figure 10, at lower $H_2O:Si$ shows a non-uniform crystal structure. As increasing the ratio to 114, the uniform and completely cubic structures are formed but when further increasing to higher ratio the crystal size are larger and have many defects.

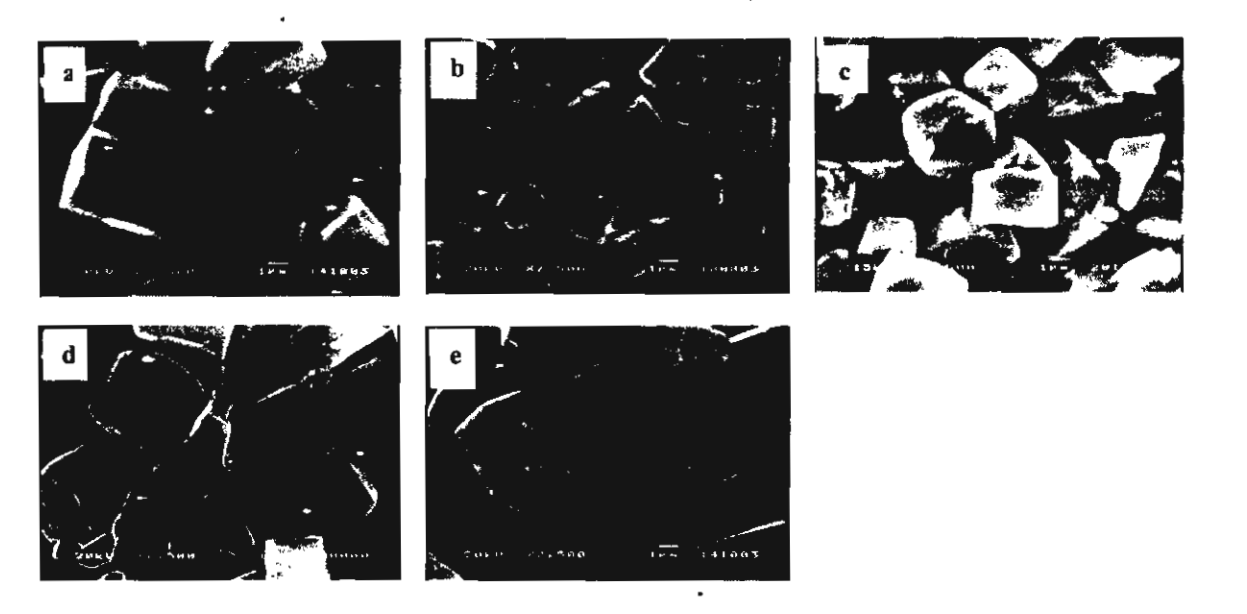


Figure 10. The SEM micrographsof TS-1 samples at various H₂O:Si molar ratios of a) 80, b) 114, c) 140, d) 170 and e) 200.

7 Effect of Si:Ti ratio

The effect of Si:Ti on the crystallization of TS-1 is carry out at Si:xTi:0.4NaOH:0.3TPA:114H₂O (x = 100.00, 33.33, 20.00, 14.29, 10.00, 7.69, 5.88 and 5.0). The reaction temperature is 150°C, aging time 110h and reaction times are varied from 15 to 35 h depending on the Ti loading (Table 1). We find that at high Ti loading, increasing the reaction time leads to the higher Ti incorporation. Figure 11 illustrates the FT-IR spectra of TS-1 samples A-H. The peak at 960 cm⁻¹ attributes to a stretching mode of an [SiO₄] unit bonded to a Ti⁴⁺ ion. (O₃SiOTi)¹² represents the incorporation of titanium in the MFI framework. A strong band at 550cm⁻¹ is the characteristic of MFI structure⁸. The DR-UV spectra of the samples A-H are shown in figure 12. The strong peak at 210 nm has been assigned to the tetra-coordinate of titanium in the zeolite framework. The broad band peak at 280 nm indicates the partially

polymerized hexa-coordinated Ti species, which contain Ti-O-Ti and belong to a silicon-rich amorphous phase¹⁹. The band at 330 nm, which assigns to the extra-framework anatase phase, is shown as a little peak in sample H. The peaks at both 210 and 280 nm are increase from sample A to H as higher titanium content and the band shift to higher wavelengths at sample with lower Si/Ti ratio because of the higher proportion of hexa-coordinate species. The peak at 280 nm increases stronger than 210 nm at sample F that means the hexa-coordinated Ti species will form at higher titanium loaded. The SEM micrograph and XRD of TS-1 samples A-H are shown in figures 13 and 14, all of the samples show the characteristic of TS-1 zeolite with the MFI structure.

Table1 The TS-1 samples at varies Si:Ti molar ratios and reaction time (h).

Sample	Si/Ti molar ratio	Reaction time (h)
a	100.00	15
b	33.33	15
c	20.00	20
d	14.29	25
e	10.00	- 25
f	7.69	35
g	5.88	35
h	5.00	35

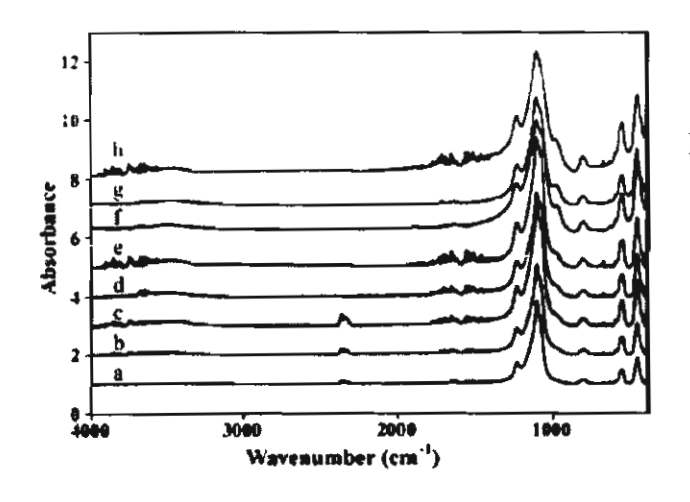


Figure 11 The FT-IR spectra of TS-1 sample at various Si:Ti molar ratios of a) 100.00, b) 33.33, c) 20.00, d) 14.29, e) 10.00, f) 7.69, g) 5.88 and h) 5.00.

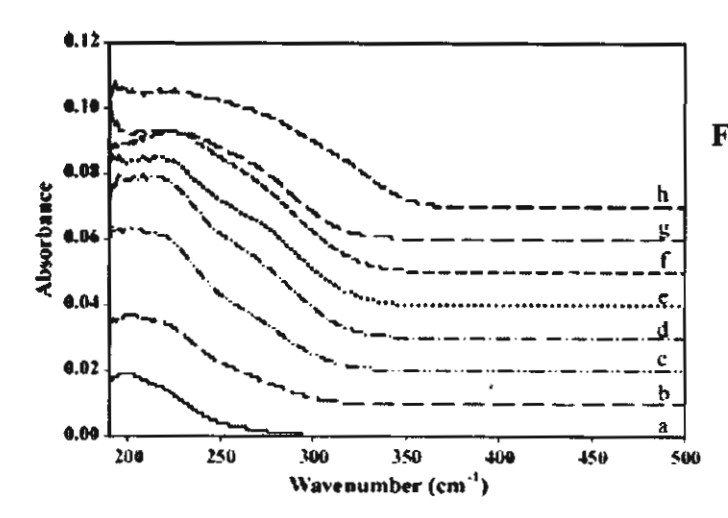


Figure 12 The DR-UV spectra of TS-1 sample at various Si:Ti molar ratios of a) 100.00, b) 33.33, c) 20.00, d) 14.29, e) 10.00, f) 7.69, g) 5.88 and h)

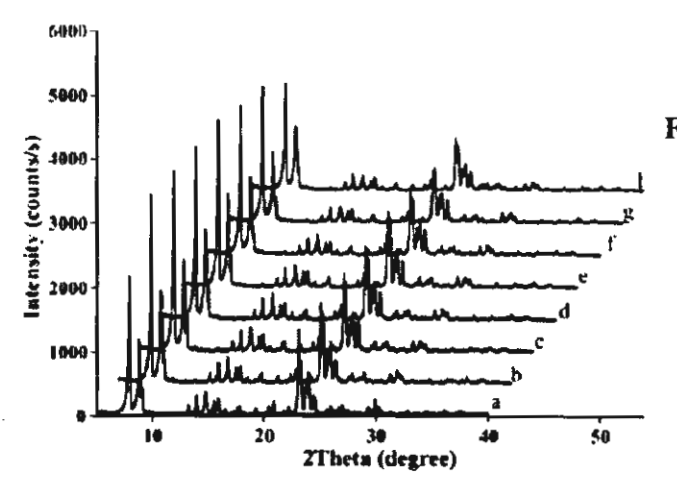


Figure 13 The XRD pattern of TS-1 sample at various Si:Ti molar ratios of a) 100.00, b) 33.33, c) 20.00, d) 14.29, e) 10.00, f) 7.69, g) 5:88 and h) 5.00.

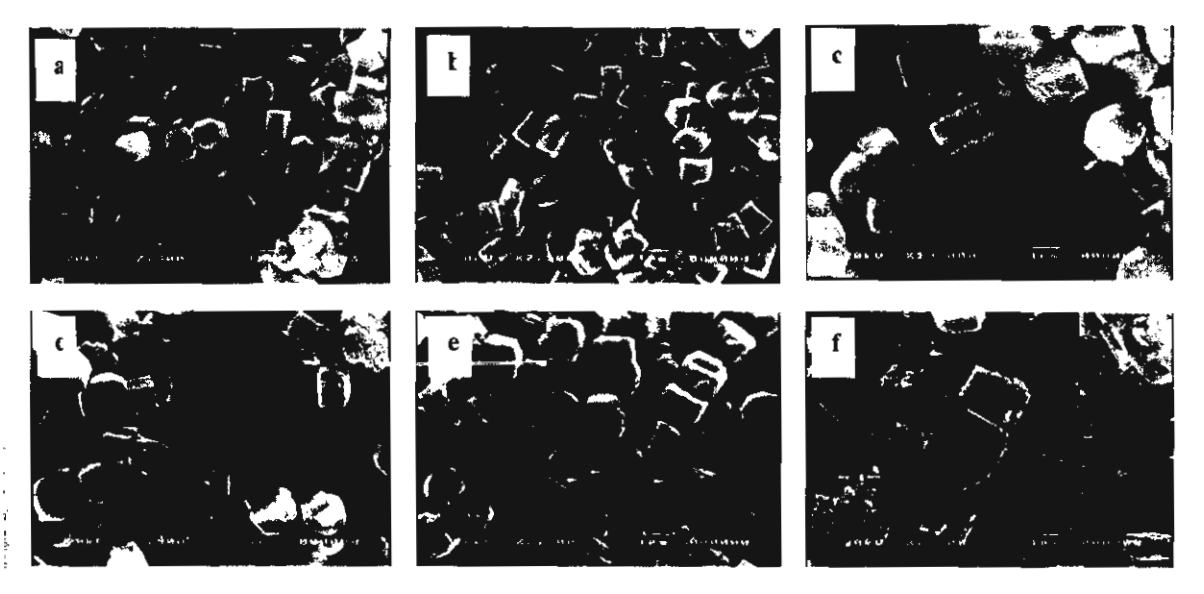


Figure 14 The SEM micrograph of TS-1 sample at various Si:Ti molar ratios of a) 100.00, b) 33.33, c) 20.00, d) 14.29, e) 10.00, f) 7.69, g) 5.88 and h) 5.00.

Photocatalytic decomposition of 4-nitrophenol

From the discussion of Lee *et al* and Lea *et al*.²⁰⁻²¹, the photocatalytic decomposition of 4-NP was completely in the presence of H₂O₂ and UV irradiation. The photodecomposition of 4-NP is governed by *OH radical reactions. The *OH can be easily to formed from titanium-hydroperoxide species. Thus, in our work we carried out the PCD of 4-NP at 1.0 mmol/l of H₂O₂ under UV irradiate. Table 2 shows the results from PCD of 4-NP with TS-1 zeolite at various Si/Ti molar ratios. The PCD increases with the amount of titanium incorporated in the zeolite and the fastest complete decomposition is at 5.0 Si:Ti molar ratio.

Table2 Photocatalytic degradation of 4-nitrophenol

Si/Ti (molar	Time for completely photocatalytic decomposition of 4-NP (h)	
ratio)		
100.00	4.00	
14.29	2.00	
7.69	1.30	
5.00	1.00	

Conclusions

The TS-1 with highly titanium incorporated in the zeolite framework was synthesized from low cost and moisture-stable precursors, silatrane and titanium glycolate, under microwave instrument. The effect of the compositions (TPA⁺, NaOH and H₂O) and conditions (aging time, reaction time and reaction temperature) were studied. The suitable condition for synthesizing TS-1 Si:0.1Ti:0.4NaOH:0.3TPA:114H₂O at aging time 110h, reaction time 15h and reaction temperature 150°C. The Si:Ti molar ratio 100.00-5.00 was studied and the results from XRD, FT-IR, SEM and DR-UV indicated that from this route highly crystalline and the Ti atoms are occupying in the zeolite framework. The reaction times were varied at different Ti loaded, which at higher titanium loading the higher reaction time was an important factor. The photocatalytic decomposition of 4-NP was used to test the activity

of prepared TS-1 samples. The samples showed high efficiency in PCD of 4-NP and the PCD increased with amount of titanium loading.

References

- Y.G. Li, Y.M. Lee, J.F. Porter, Journal of materials science 37 (2002) 1959-1965.
- 2. R.J. Davis, Z. Liu, Chemistry of Material 9 (1997) 2311-2324.
- 3. R.B. Khomane, B.D. Kulkarni, A. Paraskar, S.R. Sainkar, *Materials Chemistry and Physics* 76 (2002) 99-103.
- 4. M. Taramasso, G. Perego, B. Notari, US Patent 4410501 (1983).
- M.R. Prasad, G. Kamalakar, S.J. Kulkarni, K.V. Raghavan, K.N. Rao, P.S. Sai Prasad, S.S. Madhavendra, *Catalysis Communication* 3 (2002) 399-404.
- 6. X-S. Wang, X-W. Guo, Catalysis today 51 (1999) 177-180.
- K. Kunii, K. Narahara, S. Yamanaka, Microporous and Mesoporous Materials 52 (2002) 159-167.
- 8. S. Komarneni, A.S. Bhalla, Journal of Porous Materials 8 (2001) 23-35.
- a) P. Piboonchaisit, S. Wongkasemjit and R. Laine, "A Novel Route to Tris(silatranyloxy-i-propyl)amine Directly from Silica and Triisopropanolamine", Sci. Asia, 25, 113-119 (1999); b) N. Phonthammachai, T. Chairassameewong, E. Gulari, A.M. Jamieson, S. Wongkasemjit, J. Met. Mat. Min. 12 (2002) 23.
- 10. Q.H. Xia, Z. Gao, Materials Chemistry and Physics 47 (1997) 225-230.
- 11. G.L. Marra, G. Artioli, A.N. Fitch, M. Milanesio, C. Lamberti, *Microporous and mesoporous Materials* 40 (2000) 85-94.
- 12. J.L. Grieneisen, H. Kessler, E. Fache, A.M. Le Govic, *Microporous and Mesoporous Materials* 37 (2000) 379-386.
- D.P. Serrano, M.A. Uguina, G.Ovejero, R.V. Grieken, M. Camacho, Microporous Materials 4 (1995) 273-282.
- M.R. Boccuti, K.M. Rao, A. Zecchina, G. Leofanti, G. Petrini, Structure and Reactivity of Surfaces 48 (1989) 133-144.
- B.L. Newalkar, J. Olanrewaju, S. Komarneni, Chemistry of Materials 13 (2001) 552-557.

- C.S. Cundy, J.O. Forrest, R.J. Plaisted, Microporous and Mesoporous Materials 66 (2003) 143-156.
- 17. J.H. Koegler, H.V. Bekkum, J.C. Jansen, Zeolites 19 (1997) 262-269.
- M.A. Uguina, D.P. Serrano, G. Ovejero, R.V. Grieken, M. Camacho, Applied Catalysis A 124 (1995) 391-408.
- T. Blasco, M.A. Camblor, A. Corma, J. Perez-Pariente, Journal of American Chemical Society 115 (1995) 11806-11813.
- G.D. Lee, S.K. Jung, Y.J. Jeong, J.H. Park, K.T. Lim, B.H. Ahn, S.S. Hong, Applied Catalysis A 239 (2003) 197-268.
- 21. J. lea, A.A. Adesina, Journal of Techol Biotechnol 76 (2003) 803-810.

CHAPTER VII

PHOTOCATALYTIC MEMBRANE REACTOR OF A NOVEL HIGH SURFACE AREA TiO₂

Abstract

Photocatalytic membranes were successfully prepared using an efficient TiO₂ catalyst with high surface area, dispersed into different polymeric matrices, viz. cellulose acetate, polyacrylonitrile and polyvinyl acetate. The catalyst was directly synthesized using titanium triisopropanolamine as precursor. The membranes were characterized using FT-IR, SEM and their photocatalytic performance was tested, viz. stability, permeate flux and photocatalytic degradation of 4-nitrophenol (4-NP). We find that polyacrylonitrile provides the most effective matrix, showing the highest stability and the lowest permeate flux. The amount of TiO₂ loaded in the membrane was varied between 1, 3 and 5 wt% to explore the activity and stability of membranes in the photocatalytic reaction of 4-NP. As expected, the higher the loading of TiO₂ loaded, the higher the resulting catalytic activity.

Introduction

Purification of industrial wastewater has become an increasingly important issue, and many researchers are engaged in developing methodology to obtain efficient, low cost wastewater treatment to render harmless of all toxic species present without leaving hazardous residues. Many technologies developed for wastewater treatment, including air stripping, the use of granular activated carbon, biological degradation¹, chemical oxidation and heterogeneous photocatalysis²⁻³, have been demonstrated to be effective for complete mineralization of many toxic, bacteria and bio-resistant organic compounds in wastewater under mild experimental conditions⁴⁻⁷. The heterogeneous photocatalysis process harnesses radiant energy from natural or artificial light sources to degrade organic pollutants into their mineral components8. TiO2 is a well-established catalyst for photocatalytic degradation due to its combination of high activity, chemical stability and non-toxic properties. Photocatalytic degradation generally occurs via production of OH° radicals. When semiconductive TiO2 is illuminated by radiation of appropriate energy, electrons and holes are generated within the TiO2 structure. In the presence of O2, OH radicals are formed by reaction between the valence band holes and activated OH groups, e.g from adsorbed H2O on the TiO2 surface. To accelerate the oxidation reaction, efficient scavenging of e by O2 is necessary. The organic pollutant is attacked by hydroxyl radicals and generates organic radicals or intermediates 9-12. The main drawback to practical implementation of the photocatalysis method arises from the need for an expensive liquid-solid separation process, due to the formation of milky dispersions upon mixing the catalyst powder with water¹³.

Currently, this drawback is solved by the use of a TiO_2 membrane, consisting of fine TiO_2 particles dispersed in a porous matrix. Such titania membranes have attracted a great deal of attention in recent years due to their unique characteristics, including high water flux, semiconducting properties, efficient photocatalysis and chemical resistance relative to other membrane materials, such as silica and γ -alumina¹⁴.

Many techniques have been explored for the fixation of titania powder, including sputtering on glass, silicon or alumina¹⁵, coating via sol-gel processing on porous stainless steel plate, α-Al₂O₃ or zeolites¹⁶⁻¹⁹ were studied. However, the use of mixed matrix membranes (MMM), i.e. membranes containing microencapsulated TiO₂, becomes of increasing interest because of their high selectivity combined with outstanding separation performance, processing capabilities, and low cost, when

polymers are used as the matrix. Many researchers²⁰⁻²⁷ have explored ways to develop and facilitate the separation process, using very thin microencapsulated membranes to allow for high fluxes. Such a membrane must have a high volume fraction of homogeneously distributed encapsulated particles in a defect- and void-free polymer matrix²⁸. Polymeric membranes are not appropriate for use in membrane reactor applications where high temperatures are needed for reaction. Thus, application of MMM for catalysis of low temperature reactions has become a main topic for many researchers, for examples, hydrogenation of propyne²⁹, photomineralization of nalkanoic acids³⁰, wet air oxidation of dyeing wastewater, and photocatalytic oxidations³¹⁻³⁴.

To obtain a high photocatalytic activity, the surface area of catalyst is very important. Thus, in our work, thermally stable TiO₂ with high surface area is synthesized from moisture-stable titanium triisopropanolamine. The performance of this material as a component of an MMM was evaluated in a photocatalytic membrane reactor, using 4-nitrophenol as a model substrate, with regard to stability tests, effect of membrane type (PAN, PVac, CA), and TiO₂ loading. A comparison is made between as-prepared and commercial TiO₂.

Experimental

Materials

Titanium dioxide (surface area 12 m²/g) was purchased from Sigma-Aldrich Chemical Co. Inc. (USA) and used as received. Ethylene glycol (EG) was purchased from Malinckrodt Baker, Inc. (USA) and purified by fractional distillation at 200°C under nitrogen atmosphere before use. Triethylenetetramine (TETA) was purchased from Facai Polytech. Co. Ltd. (Bangkok, Thailand) and distilled under vacuum (0.1 mm/Hg) at 130°C prior to use. Triisopropanolamine (TIS) and 4-nitrophenoi were purchased from Sigma-Aldrich Chemical Co. Inc. (USA).

Titanium tri-isopropanolamine precursor preparation

A mixture of TiO₂ (2g, 0.025 mol), TIS (9.55g, 0.05 mol) and TETA (3.65g, 0.0074 mol) was stirred vigorously in excess EG (25 cm³) and heated to 200°C for 24 h. The resulting solution was centrifuged to separate the unreacted TiO₂. The excess EG and TETA were removed by vacuum distillation at 150°C to obtain a crude precipitate.

The product was characterized using FTIR, FAB⁺-MS and TGA. Fourier transform infrared spectra (FT-IR) were recorded on a VECOR3.0 BRUKER spectrometer with a spectral resolution of 4 cm⁻¹. Thermal gravimetric analysis (TGA) was carried out using a Perkin Elmer thermal analysis system with a heating rate of 10°C/min over 30°-800°C temperature range. The mass spectrum was obtained on a Fison Instrument (VG Autospec-ultima 707E) using the positive fast atomic bombardment mode (FAB⁺-MS) with glycerol as the matrix, cesium gun as initiator, and cesium iodide (CsI) as a standard for peak calibration.

High surface area TiO2 preparation

After removal of any excess solvent from titanium triisopropanolamine precursor, the precursor was transferred to a crucible and calcined at 600°C for 2h at heating rate of 0.25°C/min. The white powder was ground and stored in a desiccator for further use.

Membrane preparation

Polyacrylonitrile membrane

A 10 wt% mixture of polyacrylonitrile powder in dimethyl formamide (DMF) was vigorously stirred at 50°C until homogeneous. A specified amount of TiO₂ was added to the stirred polymer solution. Partial vacuum was applied for a brief duration to ensure the removal of air bubbles. The mixture was then coated on a clean glass plate using a casting knife. The resulting membrane was allowed to set for 2 min before being dried in a vacuum oven at 40°C overnight following by 60°C for 2h and 80°C for 2h. The prepared membrane was cut into a circular shape with a diameter of 6 cm and thickness of 15 μm.

Cellulose acetate membrane

The membrane preparation was followed Kunprathippanja's method³². To a suspension of TiO₂, cellulose acetate was added. A partial vacuum was applied for a brief duration to ensure the removal of air bubbles, while the suspension was stirred to obtain a homogeneous suspension. The solution was then coated on the surface of a clean glass plate. The membrane was allowed to set for 2 min, followed by submersion in an ice water bath for 2 min. The membrane was then soaked in a hot water bath at 90°C for 1h before being dried. The obtained membrane was cut into a circular shape with a diameter of 6 cm and thickness of 15 μm.

Polyvinyl acetate membrane

The polymer was dissolved at 50°C in tetrahydrofuran (THF) and stirred until all the polymer had dissolved in the solvent. TiO₂ was then added to the stirring polymer solution, followed by degassing to remove air bubbles. The mixture was transferred to a teflon flat sheet and cast to the desired thickness. The prepared membrane was left overnight at room temperature to slowly evaporate solvent and then dried in a vacuum oven at 40°C for 2h. The membrane was cut into a circular shape with a diameter of 6 cm and thickness of 15 µm.

Stability test of prepared membranes

The prepared polymeric membranes (PAN, CA and PVAc) were placed in the membrane reactor and irradiated under UV irradiation for 15 h. The concentration of 4-NP used was 140 ppm. The samples were withdrawn and analyzed for total organic carbon (TOC) to verify that the organic components were released from the prepared membrane. SEM was used to investigate the presence of defects in membranes before and after the stability test.

Photocatalytic decomposition of 4-nitrophenol

The photocatalytic reactions were carried out in a 500 ml continuous batch glass reactor, figure 1, with a gas inlet and outlet at an O₂ flow rate of 20 ml/min. A cooling water jacket was used to maintain the temperature at 30°C. The suspensions and membrane were illuminated using a 100 Watt Hg Philip UV lamp. The concentration of 4-NP used was 140 ppm and the solution was continuously stirred. The obtained permeate was removed at 1h intervals and analyzed to determine the concentration of 4-NP using a Shimadzu UV-240 spectrophotometer.

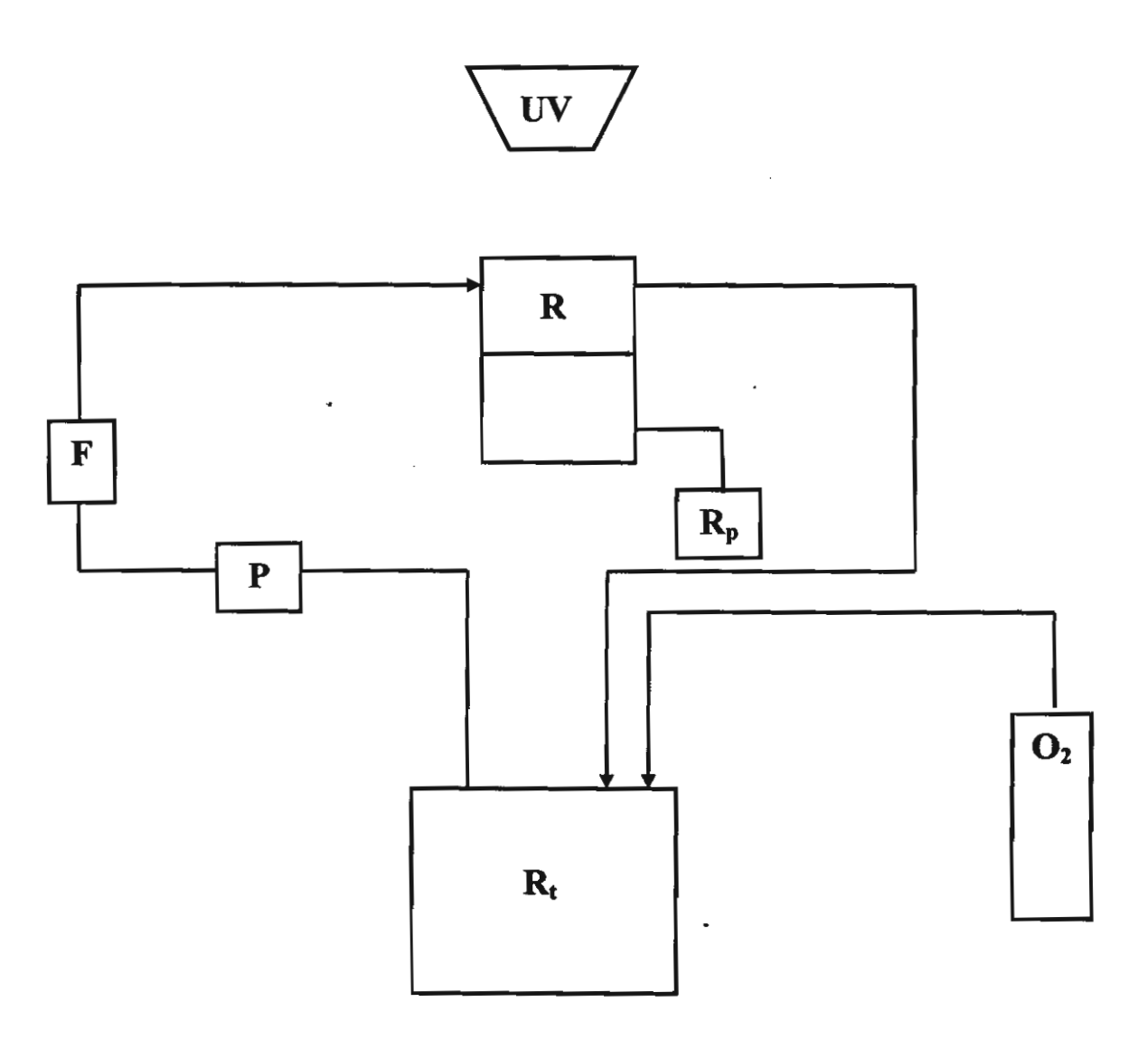


Figure 1 The schematic diagram of photocatalytic membrane reactor (F, flowmeter; R, reactor; R_p, permeate reservoir; R_t, recirculating tank and P, peristaltic pump).

Titanium triisopropanolamine and TiO2 catalyst characterization

High surface area TiO₂ was characterized by various techniques. The XRD pattern was obtained using a D/MAX-2200H Rigaku diffractometer with CuKα radiation on specimens prepared by packing sample powder into a glass holder. The diffracted intensity was measured by step scanning in the 2θ range of 5° to 90°. Fourier transform infrared spectra (FT-IR) were recorded on a VECOR3.0 BRUKER spectrometer with a spectral resolution of 4 cm⁻¹. Samples pyrolyzed at 600°C were analyzed using SEM by attachment onto aluminum stubs after coating with gold via vapor deposition. Micrographs of the pyrolyzed sample surfaces were obtained at

x7,500 magnification. Specific surface area and nitrogen adsorption-desorption were determined using an Autosorp-1 gas sorption system (Quantachrome Corporation) via the Brunauer-Emmett-Teller (BET) method. A gaseous mixture of nitrogen and helium was allowed to flow through the analyzer at a constant rate of 30 cc/min. Nitrogen was used to calibrate the analyzer, and also as the adsorbate at liquid nitrogen temperature. The samples were thoroughly outgassed for 2h at 150°C, prior to exposure to the adsorbent gas.

Membrane characterization

Three different types of membranes made from PAN, CA and PVAc were characterized using SEM, FT-IR and DR-UV. The morphology of membranes was analyzed by attachment onto aluminum stubs and coated with gold via vapor deposition. The membranes were frozen in liquid nitrogen and fractured to examine the cross-sectional areas. The samples were characterized on a JEOL 5200-2AE(MP 15152001) scanning electron microscope. Fourier transform infrared spectra (FT-IR) were recorded on a VECOR3.0 BRUKER spectrometer with a spectral resolution of 4 cm⁻¹ using transparent KBr pellets containing 0.001 g of sample mixed with 0.06 g of KBr. The samples were also analyzed to determine the amount of TiO₂ using a Shimadzu UV-240 spectrophotometer.

Results and discussion

Titanium triisopropanolamine precursor characterization

The synthesized titanium triisopropanolamine was characterized using FT-IR, TGA, MS and SEM. The IR spectrum (fig 2.) of the product shows bands at 3400 cm⁻¹ (OH group), 2927-2855 cm⁻¹ (C-H stretching), 1460 cm⁻¹ (C-H bending of CH₂ group), 1379 cm⁻¹ (C-H bending of CH₃ group), 1085 cm⁻¹ (C-O-Ti stretching), 1020 cm⁻¹ (C-N bending) and 554 cm⁻¹ (Ti-O stretching). The TGA thermogram, as seen in figure 3, shows two transitions, at 280° and 365°C, corresponding to the decomposition of unreacted triisopropanolamine and the triisopropanolamine ligand, respectively, reflecting the use of excess triisopropanolamine in the reaction and no purification of the obtained product. The final ceramic yield of the product was calculated from the starting point of the second decomposition transition, and was found to be 16.60%, close to the theoretical ceramic yield of 18.65%. The results of mass spectral analysis, summarized in table1, confirm the prepared sample has the desired structure.

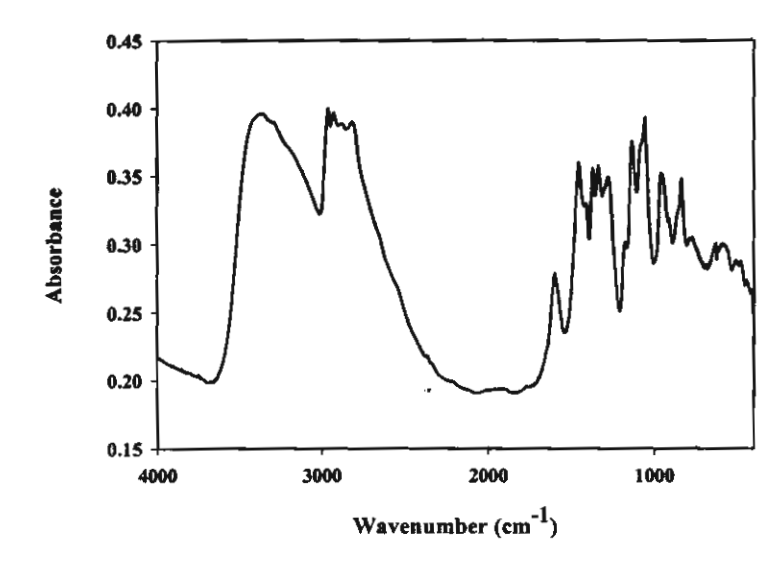


Figure 2 FT-IR spectrum of titanium triisopropanolamine.

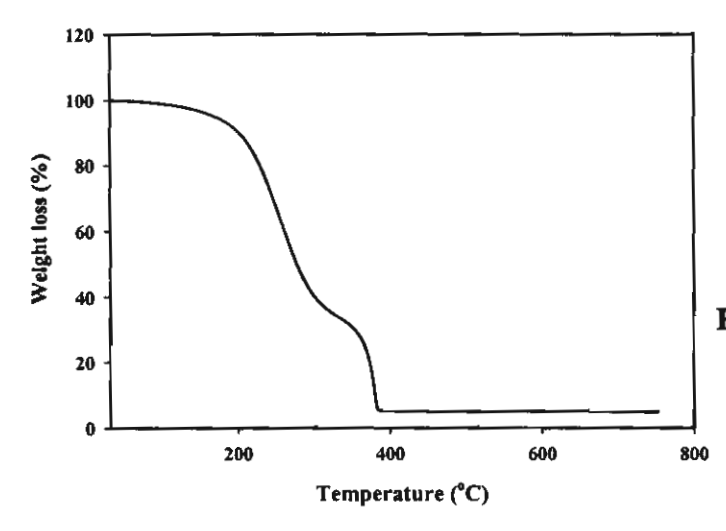


Figure 3 TGA thermogram
of titanium
triisopropanolamine.

Table 1 The proposed structure and fragments of the synthesized titanium triisopropanolamine.

M/e	%intensity	Proposed structure	
428	10	H ⁺ [HOCH ₃ CHCH ₂]N[CH ₂ CH ₃ CHO] ₂ Ti[OCHCH ₃ CH ₂] ₂ N[CH ₂ CHCH ₃ OH]H ⁺	
410	5	[CH ₃ CH ₂ CH ₂]N[CH ₂ CHCH ₃ O] ₂ Ti[OCHCH ₃ CH ₂] ₂ N [CH ₂ CHCH ₃ OH]	
214	58	[H ₂ NCHCH ₃ CH ₂ O] ₂ Ti[OH]	
192	100	H+N[CH ₂ CHCH ₃ OH] ₃	

TiO₂ catalyst characterization

The calcined product was characterized using XRD, BET surface area and SEM to confirm the presence of the active anatase phase of TiO_2 . The XRD pattern shown in fig. 4, exhibits diffraction peaks at $2\theta = 25.28$, 37.66, 47.90, 54.64, 62.58, 69.76, 75.26 and 82.72, and the particle morphology (fig. 5) shows irregularly-shaped particles, characteristic of the anatase phase of TiO_2 , as previously reported³⁵. The surface area measurement of a sample calcined at 600°C for 2h shows a high surface area of 163 m²/g. Also, the nitrogen adsorption-desorption isotherm of this material exhibits type IV character (fig. 6.) indicative of a mesoporous structure.

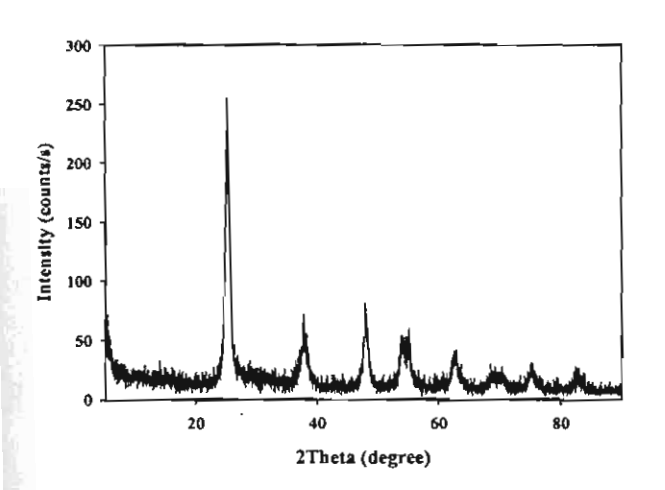


Figure 4 XRD pattern of the anatase phase of the prepared TiO₂ catalyst calcined at 600°C for 2h.

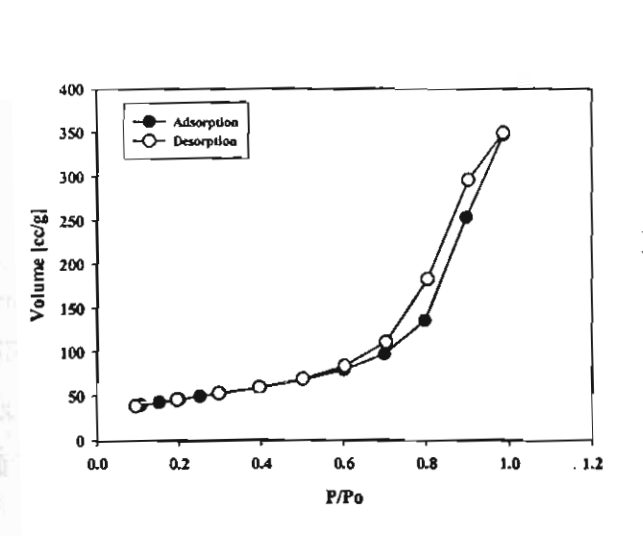




Figure 5 SEM micrograph of the anatase phase of the prepared TiO₂ catalyst calcined at 600°C for 2h.

Figure 6 Nitrogen adsorption

desorption isoterm for the

prepared mesoporous titania

calcined at 600°C

Membranes characterization

The prepared mixed matrix membranes were characterized with respect to their functional groups using FT-IR, their morphology using scanning electron microscopy (SEM) and the amount of TiO₂ loaded in the membrane using diffuse reflectance UV. The membrane stability test was also carried out to demonstrate that the obtained material is suitable for use as a membrane.

The FT-IR spectrum of CA (fig. 7a) shows the characteristic abscrption bands of C=O, C-O-C and C-C bonds at 1780, 1174 and 1020 cm⁻¹, respectively. The peak in the region of 800-500 cm⁻¹ is associated with the vibration of the Ti-O bond²⁵. For the PAN membrane (fig 7b), the band at 2260 cm⁻¹ is characteristic of the CN bond while the spectrum of PVAc in fig. 7c shows bands at 1780 and 1200 cm⁻¹ representing the C=O and C-C bonds, respectively.

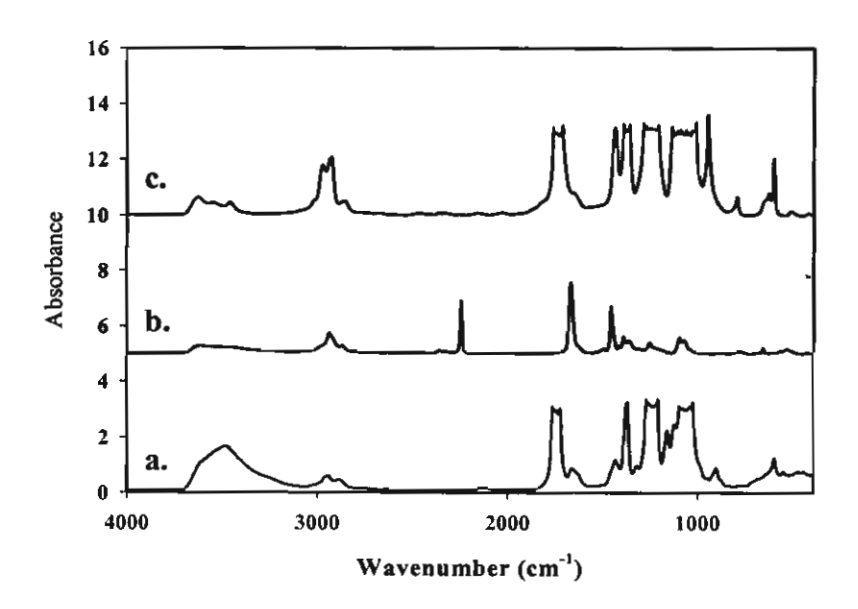


Figure 7 FT-IR spectra of the prepared membranes using 1wt%TiO₂ mixed in a). cellulose acetate, b), polyacrylonitrile and c), polyvinyl acetate.

SEM micrographs of the fracture surfaces of all three types of membranes are shown in figure 8. The CA membrane (fig. 8a.) presents a porous surface distinctly different from the surfaces of PAN and PVAc (fig.8b. and 8c.). The TiO₂ particles are immobilized within the polymeric matrix. No significant loss of particles was observed during the membrane formation process on the glass plate. The micrographs reveal no

evidence for the presence of voids between the polymer and TiO₂. TiO₂ particles are well distributed across the surface and do not agglomerate.

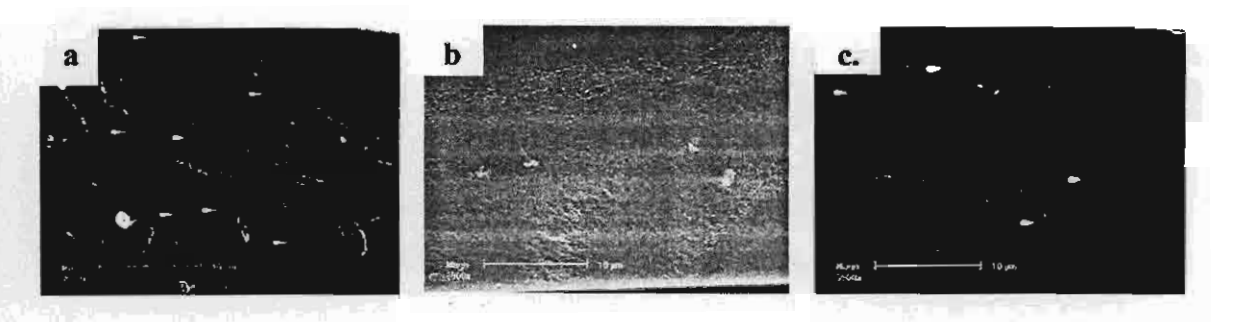


Figure 8 SEM micrographs of mixed matrix membranes using a.) cellulose acetate, b.) polyacrylonitrile and c.) polyvinyl acetate.

The PAN membrane type was selected to study the effect of TiO₂ loading, varying the percentage of TiO₂ between 1, 3 and 5 wt%. Figure 9 shows the DR-UV spectra of the prepared membranes. As expected, the absorbance at 320 nm, which is characteristic of TiO₂, increases with the amount of TiO₂. Morphological analysis by SEM, shown in fig. 10, indicates that TiO₂ particles are well dispersed throughout the PAN matrix at all loadings.

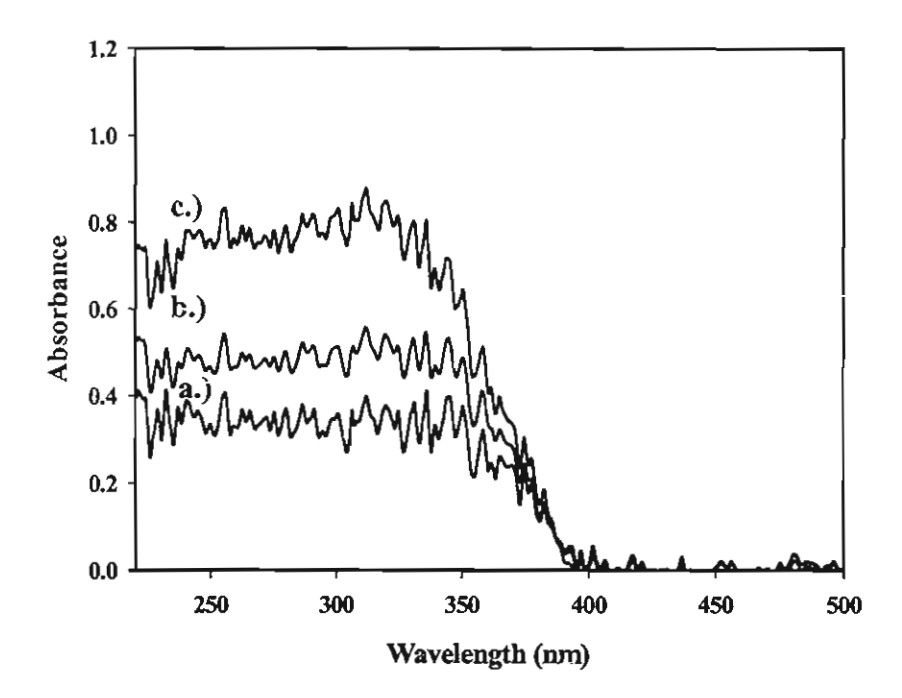


Figure 9 DR-UV spectra of polyacrylonitrile membranes at various percentages of TiO₂; a) 1, b) 3 and c) 5wt%.



Figure 10 SEM micrographs of polyacrylonitrile membranes at various percentages of TiO₂; a) 1, b) 3 and c) 5wt%

The stability of the prepared membranes was tested using UV illumination and exposure to 4-NP for 15h, and evaluation by TOC, as summarized in table 2. The PAN and CA membranes were stable under these conditions, as indicated by essentially no change in TOC values. However, the PVAc membrane showed a higher TOC value, indicative that the PVAc membrane was not stable and undergoes decomposition.

 Table 2
 The stability tests of the prepared membranes.

Membrane type	TOC (at initial)	TOC (after 15h)
PAN	22.39	22.68
CA	22.63	22.57
PVAc	22.35	32.22

Photocatalytic degradation of 4-nitrophenol

The photocatalytic activities of the three membrane types were assessed using the photoreactor shown in fig. 1, employing 1 wt% immobilized photocatalyst TiO₂, oxygen flow rate of 20 ml/min. 4-NP flow rate of 30 ml/min and 4-NP concentration of 140 ppm. The permeation flux data (fig. 11) shows that CA and PAN membranes have constant low permeate flux levels, 12.38 and 5.31 l/h m², respectively, whereas the PVAc membrane shows a steep increase in permeate flux from 10.62 to 120 l/h m² as reaction time increases from 1 to 2h. The higher permeate flux of CA membrane than PAN is consistent with the SEM observation in fig. 8, that the CA membrane is more porous than the PAN membrane. The dramatic increase in permeate flux of the PVAc membrane occurs because of the decomposition of this membrane, which generates

defects during the reaction, as confirmed by the SEM micrograph in figure 12. The holes generated in the polymer matrix cause an increase in the flux and a decrease in the photodegradation activity. The efficiencies of the PAN and CA membranes for photocatalytic degradation of 4-NP are illustrated in fig. 13, which indicates, at 1 wt% Ti loading, no substantive differences in the rate of degradation of 4-NP between the PAN and CA membranes. During the first hour of UV illumination, the concentration of 4-NP permeating through the PAN membrane is higher than through the CA membrane. This is unexpected and may reflect experimental uncertainty, since, in view of the higher permeate flux of the CA membrane, more 4-NP molecules should penetrate through the CA membrane. However, after 7hr of illumination, each membrane shows similar activity, as expected at such low TiO₂ loadings. For the PVAc membrane, the reaction could not be monitored through 7hr because the defects produced by degradation causing an extremely high flux, as discussed above.

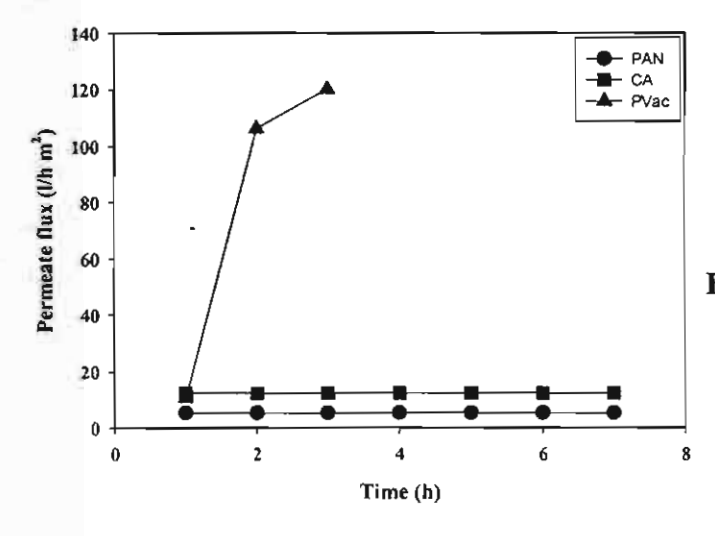


Figure 11 The permeate flux versus reaction time of all three types of the prepared membranes.



Figure 12 SEM micrograph
showing the defect of
polyvinyl acetate membrane
after the reaction.

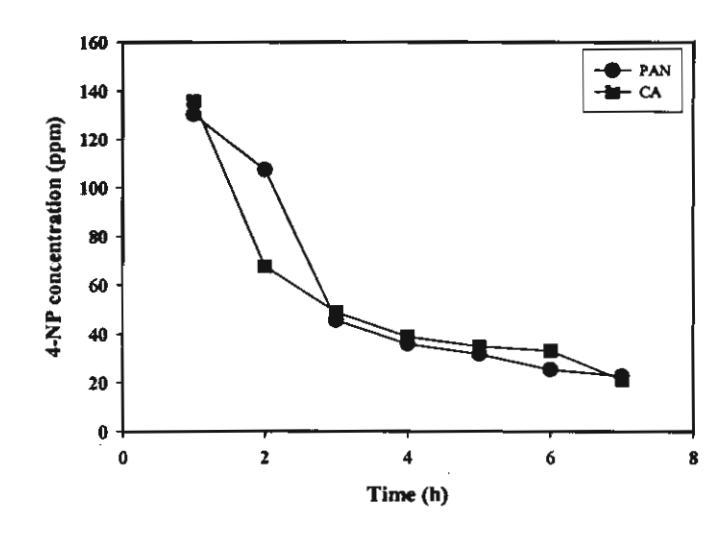


Figure 13 The degradation of 4
NP with the reaction time of polyacrylonitrile and cellulose acetate membranes.

Effect of various amounts of TiO_2 in PAN membrane on the photocatalytic degradation of 4-nitrophenol

The PAN membrane was selected to investigate the effect of TiO₂ loading on the efficiency of photocatalytic degradation because of its stability and the fact that it exhibits the lowest permeant flux. Figure 14 shows the permeant flux of PAN membranes at the three loading levels, 1, 3 and 5 wt% of TiO₂. We find that the flux is constant for all three samples, and increases with the amount of TiO₂ from 5.31, to 8.13 to 12.73 l/h m², respectively. In fig. 15, the efficiency of degradation of 4-NP at the three loading levels of TiO₂ is reported. Initially, the decrease of 4-NP at 3 and 5% loadings appears to be faster than at 1%. As for Fig. 13, however, this may be experimental error. At long times, there appears to be no significant differences in the concentrations of 4-NP measured. The reason may be that the percentage of TiO₂ is too low to see any differences in the degree of degradation of 4-NP. However, when compared with literature results³⁴, performed at much higher loading levels of TiO₂, it appears that these membranes show a higher level of catalytic activity.

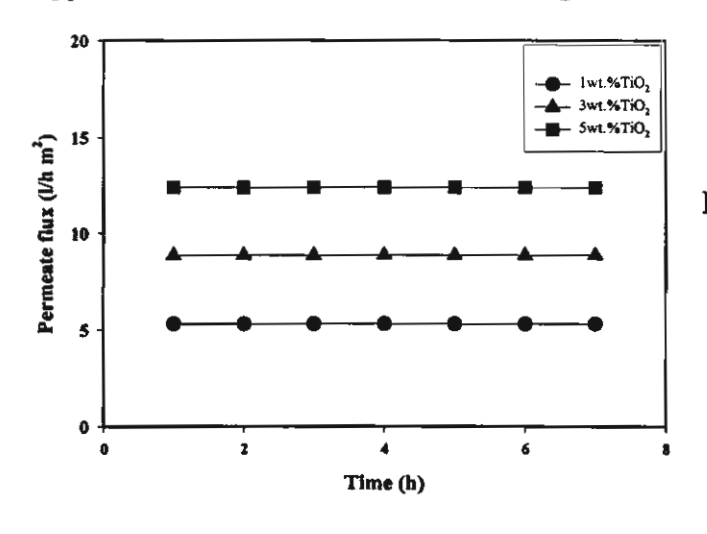


Figure 14 The permeate flux versus reaction time of polyacrylonitrile membranes at various percentages of TiO₂.

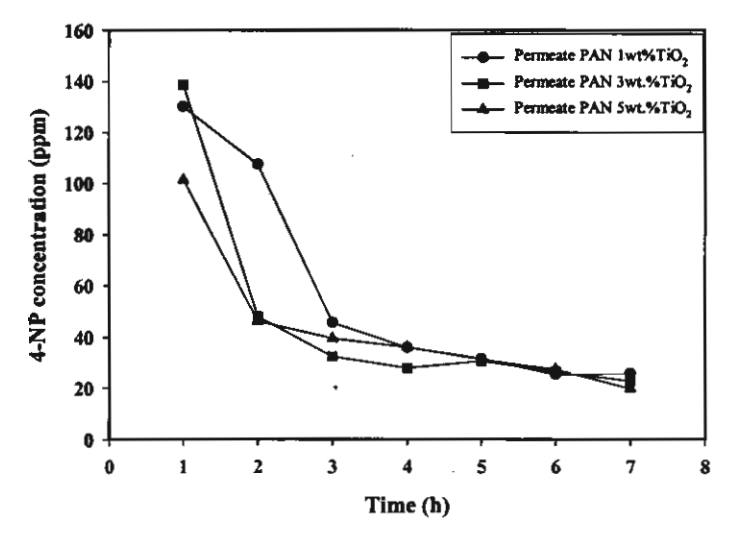


Figure 15 The degradation of 4-NP with the reaction time of polyacrylonitrile membranes at various percentages of TiO₂.

Commercial TiO₂ (Degussa P25) is also studied to compare with our TiO₂ at loading level of 3wt%. The result, see fig. 16, indicates no permeation of 4-NP through membrane prepared using commercial TiO₂ and the efficiency of degradation of 4-NP measured from the retentate of two membranes shows that the degradation of 4-NP in the membrane prepared using our TiO₂ is distinguishably lower.

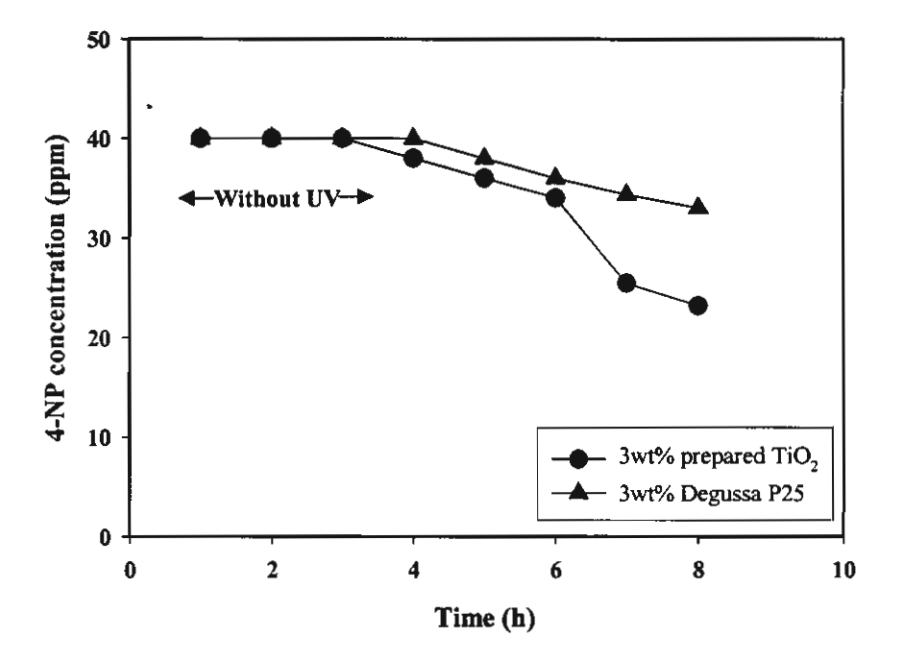


Figure 16 Effect of TiO₂ type mixed in the polyacrylonitrile membrane on the degradation of 4-NP.

Conclusions

The titanium triisopropanolamine precursor can be prepared by a very simple method (the oxide one pot synthesis) from low cost starting materials, and yields a TiO₂ catalyst with high surface area was obtained after calcinations of the precursor at 600°C for 2h. Polymeric membranes loaded with the as prepared TiO₂ catalyst show an impressively high efficiency for the photocatalytic degradation of 4-NP. Examination of the properties of three different types of membrane (PAN, CA and PVAc) indicates that the highest stability and lowest permeate flux is observed with the PAN membrane and the poor stability occurs with the PVAc membrane. The photocatalytic degradation of 4-NP increases with increased percentage of TiO₂ loaded in the PAN membrane.

References

- Razo-Flores, M. Iniestra-Gonzalez, J.A. Field, P. Olguin- Lora, L. Puig-Grajales, Journal of Environmental Engineering (2003) 999-1006.
- 2. S. Zhou, A.K. Ray, Ind. Eng. Chem. Res. 42 (2003) 6020-6033.
- H. Chun, W. Yizhong, T. Hongxiao, Applied Catalysis B: Environmental 35 (2001) 95-105.
- 4. V. Loddo, G. Marci, C. Martin, L. Palmisano, V. Rives, A. Sclafani, Applied Catalysis B: Environmental 20 (1999) 29-45.
- B. Barni, A. Cavicchioli, E. Riva, L. Zanoni, F. Bignoli, I.R. Bellobono, Chemosphere 30 (1995) 1847-1860.
- P-C. Maness, S. Smolinski, D.M. Blake, Z. Huang, E.J. Wolfrum, W.A. Jacoby, Applied and Environmental Microbiology 65 (1999) 4094-4098.
- 7. A.J. Maira, W.N. Lau, C.Y. Lee, P.L. Yue, C.K. Chan, K.L. yeung, Chemical Engineering Science 58 (2003) 959-962.
- 8. D. Chen, A.K. Ray, Applied Catalysis B: Environmental 23 (1999) 143-157.
- 9. R. Villacres, S. Ikeda, T. Torimoto, B. Ohtani, Journal of Photochemistry and Photobiology A: Chemistry 160 (2003) 121-126.
- A.G. Rincon, C. Pulgarin, N. Adler, P. Peringer, Journal of Photochemistry and Photobiology A: Chemistry 139 (2001) 233-241.
- 11. A. Makowski, W. Wardas, Current topics in Biophysics 25 (2001) 19-25.
- 12. S. Liu, K. Li, Journal of Membrane Science 218 (2003) 269-277.

- D. Dumitriu, A.R. Bally, C. Ballif, P. Hones, P.E. Schmid, R. Sanjines, F. Levy,
 V.I. Parvulescu, Applied Catalysis B: Environmental 25 (2000) 83-92.
- L. Zhang, T. Kanki, N. Sano, A. Toyoda, Separation and Purification Technology 31 (2003) 105-110.
- T.V. Gestel, C. Vandecasteele, A. Buekenhoudt, C. Cotremont, J. Luyten, R. Leysen, B.V.D. Bruggen, G. Maes, Journal of Membrane Science 209 (2002) 379-389.
- P. PuhlfurB, A. Voigt, R. Weber, M. Morbe, Journal of Membrane Science 174 (2000) 123-133.
- 17. Y.S.S. Wan, J.L.H. Chau, A. Gavriilidis, K.L. Yeung, Microporous and Mesoporous Materials 42 (2001) 157-175.
- 18. J. Chen, L. Eberlein, C.H. Langford, Journal of Photochemistry and Photobiology A: Chemistry 148 (2002) 183-189.
- 19. I. Ortiz, P. Alonso, A. Urtiaga, Desalination 149 (2002) 67-72.
- K. Karakulski, W.A. Morawski, J. Grzechulska, Separation and Purification Technology 14 (1998) 163-173.
- 21. C.M. Zimmerman, A. Singh, W.J. Koros, Journal of Membrane Science 137 (1997) 145-154.
- M-E. Avramescu, Z. Borneman, M. Wessling, Journal of Chromatography A 1006 (2003) 171-183.
- 23. M. M. Clark, P. Lucas, Journal of Membrane Science 143 (1998) 13-25.
- 24. Z. Lu, G. Liu, S. Duncan, Journal of Membrane Science 221 (2003) 113-122.
- 25. Q. Hu, E. Marand, S. Dhingra, D. Fritsch, J. Wen, G. Wilkes, Journal of Membrane Science 135 (1997) 65-79.
- 26. S.B. Tantekin-Ersolmaz, L. Senorkyan, N. Kalaonra, M. Tather, A. Erdem-Senatalar, Journal of Membrane Science 189 (2001) 59-67.
- 27. A. Figoli, W. Sager, M. Wessling, Desalination 148 (2002) 401-405.
- 28. S. Ziegler, J. Theis, D. Fritsch, Journal of Membrane Science 187 (2001) 71-84.
- 29. L. Rivas, I. R. Bellobono, F. Ascari, Chemosphere 37 (1998) 1033-1044.
- 30. L. Lei, X. Hu, P.-L. Yue, Water Research 32 (1998) 2753-2759.
- 31. R. Molinari, M. Mungari, E. Drioli, A.D. Paola, V. Loddo, L. Palmisano, M. Schiavello, Catalysis Today 55 (2000) 71-78.

- 32. W. Rattanawong, S. Osuwam, T. Risksomboon, S. Kulprathipanja, American Chemical Society, Div. Pet. Chem. 46 (2001) 166-167.
- 33. M.E. Zorn, Proceeding of the 13th Annual Wisconsin Space Conference August 14-15, 2003. Green Bay, WI. Wisconsin Space Grant Consortium: 2003.
- 34. R. Molinari, L. Palmisano, E. Drioli, M. Schiavello, Journal of Membrane Science 206 (2002) 399-415.
- 35. N. Phonthammachai, T. Chairassameewong, E. Gulari, A. M. Jamieson, S. Wongkasemjit, Microporous and Mesoporous Materials 66 (2003) 261-271.

CHAPTER VIII CONCLUSIONS

Titanium glycolate and titanium triisopropanolamine are successfully synthesized using low cost starting materials, and a much simpler and milder reaction condition. The products show good property in moisture stability. The results from spectroscopy, namely, FT-IR, EA, Solid state NMR, and TGA, confirm the product structure. The transformation from anatase to rutile phases of calcined titanium glycolate indicates the anatase stability up to 900°C. The stability of the synthesized product remarkably provides researchers to make use in many applications. Anatase TiO₂ nanoparticles were successfully prepared by the sol-gel technology, using moisture-stable titanium glycolate as precursor in 1M HCl solution. The calcination temperature and the HCl:H₂O volume ratio have a substantial influence on the surface area, phase transformation and morphology of the products. Anatase titania is produced at calcination temperatures in the range of 600° to 800°C, above which transformation to rutile occurs. Increase of temperature results in anatase of higher crystallinity but lower specific surface area, and induces a morphological change from large irregular agglomerates to more homogeneous particles of spherical shape. From XRD measurements of average grain sizes, we deduce that nucleation rate dominates the kinetics at low temperatures, and growth rate becomes the controlling factor at high temperature and low HCl:H2O ratios. Increase of HCl:H2O ratio results in a small but significant decrease in porosity. The highest specific surface area 125 m²/g is obtained at the lowest HCl:H₂O ratio of 0.28 and the lowest calcination temperature (600°C). From rheological analysis, as evaluated by the Winter criteria, the gelation time increases with increase of HCl:H2O volume ratio. The fractal dimension determined from the frequency scaling exponent of the modulus at the gel point indicates a denses critical gel structure at low acid ratio. However, the complex viscosity and gel strength increase as a function of acid ratio. We interpret this behavior as indicative that, at low acidity, the gel is composed of poorly hydrated particles forming a dense but weak structure. Increase in acidity increases hydration and cross-link density leading to a more open and stronger gel network. From the rheological study of different ceria gelling system using HCl:alkoxide molar ratio of 0.8, 0.9, 1.0 and 1.1, as evaluated by Winter et al., the gelation time increases as increasing HCl:alkoxide molar ratio. The gel strength increases as a function of acid ratio and the fractal dimension determined from the frequency scaling exponent of the modulus at the gel point indicate a tight structure at low acid ratio. The TS-1 with highly titanium incorporated in the zeolite framework was synthesized from moisture-stable precursors, silatrane and titanium glycolate, under microwave treatment. The effects of the compositions (TPA⁺, NaOH and H₂O) and conditions (aging time, reaction time and reaction temperature) showed that the suitable condition for synthesizing TS-1 was Si:0.1Ti:0.4NaOH:0.3TPA:114H₂O at aging time 110h, 15h reaction time and reaction temperature of 150°C. As for the Si:Ti molar ratio, from XRD, FT-IR, SEM and DR-UV results, it is indicated that high crystallinity and the Ti atoms are occupying in the zeolite framework. Moreover, at higher titanium loading the higher reaction time was an important factor. It is also important to the photocatalytic decomposition of 4-NP. The samples showed high efficiency in PCD of 4-NP and the PCD increased with amount of titanium loading.

The titanium triisopropanolamine precursor was successfully prepared using the same method, and yields a TiO₂ catalyst with high surface area after calcinations of the crude precursor at 600°C for 2h. Polymeric membranes loaded with the as-prepared TiO₂ catalyst show an impressively high efficiency for the photocatalytic degradation of 4-NP. Examination of the properties of three different types of membrane (PAN, CA and PVAc) indicates that the highest stability and the lowest permeate flux are observed with the PAN membrane and the poor stability occurs with the PVAc membrane. The photocatalytic degradation of 4-NP increases with increasing percentage of TiO₂ loaded in the PAN membrane.

APPENDIX: Project Outputs

A. National Patent

ជាមោ

แบบ สป/สผ/อสป/003-ก หน้า 1 ของจำนวน 3 หน้า

	สำหรับเจ้าหน้าที่				
	วันรับคำขอ 19 ถึ:	เลขที่กำขอ			
	วันชิ้นคำขอ	103423			
คำขอรับสิทธิบัศร/อนุสิทธิบัศร	สัญลักษณ์จำแนกการประดิษฐ์ระหว่างประเทศ				
🖾 การประดิษฐ์	ใช้กับแบบผลิดภัณฑ์				
🗖 การออกแบบผลิตภัณฑ์	ประเภทหลิดภัณฑ์				
🔲 อนุสิทธิบัตร	วันประกาศใจษณา	เลขที่ประกาศโพษณา			
ซ้าพเข้าผู้ถงถายมือชื่อในคำขอรับสิทธิบัตร/อนุสิทธิบัตรนี้	วันออกสิทธิบัตร/อนุสิทธิบัตร	เลขที่สิทธิบัตร/อนุสิทธิบัตร			
ขอรับสิทธิบัคร/อนุสิทธิบัคร ตามพระราชบัญญัติสิทธิบัคร พ.ศ. 2522					
แก้ไขเพิ่มเดิม โดยพระราชบัญญัติสิทธิบัตร (ฉบับที่ 2) พ.ศ 2535 และ พระราชบัญญัติสิทธิบัตร (ฉบับที่ 3) พ.ศ 2542	ลาชมือชื่อเจ้าหน้าที่				
 เรื่อที่แสดงถึงการประดิษฐ์/การออกแบบผลิตภัณฑ์ 	<u> </u>				
เชื่อแผ่นสำหรับย่อยสถายสารพิษและเรื้อโรคด้วยแสง					
2.คำขอรับสิทธิบัตรการออกแบบผลิตภัณฑ์นี้เป็นคำขอสำหรับแบบผลิตภัณฑ์อย่างเคือวกับและเป็นคำขอลำคับที่					
ในจำนวน คำขอ ที่อื่นในความคือวกัน					
 ลู้ขอรับสิทธิบัคร/อนุสิทธิบัคร และที่อยู่ (เลขที่ ถนน ประเทศ) 	3.1 สัญชาติ	3.1 สัญชาติ			
ดูที่หน้า 3	3.2 โทรศัพท์				
	3.3 โทรสาร				
	3.4 อีเมล์				
4.สิทธิในการขอรับสิทธิบัตร/อนุสิทธิบัตร	<u> </u>				
🔲 ผู้ประดิษฐ์หู้ออกแบบ 🗹 ผู้รับโอน 🔲 ผู้ขอรับสิทธิ	โดยเหตุอื่น				
5.ตัวแทน(ถ้ามี) ที่อยู่ (เลขที่ ถนน จังหวัด รหัสไปรษณีย์)	5.1 ตัวแทนเลขที่ 1453				
นายบงคล แก้วบหา	5.2 โทรศัพท์ 0-2218-2	5.2 ใทรศัพท์ 0-2218-2895-6			
สถาบันทรัพธ์สินทางปัญญาแห่งจุฬาลงกรณ์มหาวิทยาลัย รั้น 9 ห้อ อาคารเทพทวาราวดี คณะนิติศาสคร์ จุฬาลงกรณ์มหาวิทยาลัย	4 904 5.3 โทรสาร 0-2215-0	5.3 โทรสาร 0-2215-0115			
อ พารเทพทราร เวพ พณะนพทากพร ชุพ เถจารอนมหารทธากอ ถนนพญาไท แขวจวังใหม่ เขตปทุมวัน กรุงเทพฯ 10330	5.4 อีเมล์	5.4 ชีเมล์			
6.ผู้ประติษฐ์/ผู้ออกแบบผลิตภัณฑ์ และที่อยู่ (เลขที่ ถนน ประเทศ)					
รองศาสตราจารย์ คร.สุจิตรา วงศ์เกษบจิตต์ และ นางสาวนพวรรณ พรธรรมชัย					
วิทยาลัยปีโดรเลียมและปีโดรเคมี จุฬาลงกรณ์มหาวิทยาลัย แขวงวังใหม่ เขตปทุมวัน ภรุงเทพฯ 10330					
7. คำขอรับสิทธิบัตร/อนุสิทธิบัตรนี้แยกจากหรือเกี่ยวข้องกับคำขยเดิม					
ผู้ขอรับสิทธิบัตร/อนุสิทธิบัตร ขอให้ถือว่าได้อื่นคำขอรับสิทธิบัตร/อนุสิทธิบัตรนี้ ในวันเดียวกับคำขอรับสิทธิบัตร					
เลขที่ วันอื่น เพราะคำขอรับสิทธิบัตร/อนุสิทธิบัตรนี้แยกจากหรือเกี่ยวข้องกับคำขอเดิมแพราะ					
🔲 คำขอเดิมมีการประดิษฐ์หลายอย่าง 🔲 ถูกลัดด้านเนื่องจากผู้ขอใน่มีสิทธิ์ 🗀 ขอเปลี่ยนแปลงประเภทของสิทธิ์					

<u>พมายมหตุ</u> ในกรณีที่ไม่อาจระบุราชละเอ็จลได้ครบด้วน ให้จัดทำเป็นเอกสารแบบท้ายแบบทีมที่นี้โดยระบุทมายเลขกำกับข้อและทัวข้อที่แสดงราชละเอ็จด เพิ่มเดิมดังกล่าวด้วย

แบบ สป/สผ/อสป๋/001-ก หน้า 2 ของจำนวน 3 หน้า

 การขึ้นคำขอนอกราชอาณาจักร 						
วันชื่นคำขอ	เถขที่คำขอ	ประเทศ	สัญลักษณ์จันเนกการ ประดิษฐ์ระหว่างประเทศ	สถานะคำขอ		
8.1		-				
8.2						
ເນ			20,000			
8.4 🔲 ผู้ขอรับสิทธิบัคร/อนุสิทธิบัครขอสิทธิให้ถือว่าได้อื่นคำขอนี้ในวันที่ได้อื่นคำขอรับสิทธิบัคร/อนุสิทธิบัครในค่างประเทศเป็นครั้งแรกโดย						
🗖 ได้ชิ้นเอกสารหลักฐานพร้อมคำขอนี้ 🔲 ขอชื่นเอกสารหลักฐานหลังจากวันชิ้มคำขอนี้						
9.การแสดงการประดิษฐ์ หรือการออกแบบผถิตภัณฑ์ ผู้ขอรับสิทธิบัตร/อนุสิทธิบัตร ได้แสดงการประดิษฐ์ที่หน่วยงานของรัฐเป็นผู้จัด						
วันแสดง	วันเปิดงานแสดง	ผู้รัก				
10.การประดิษฐ์เกี่ยวกับจุลรีพ						
10.1 เลขทะเบียนผ่ากเก็บ	10.2 วัน	ที่ฝากเก็บ	10.3 สถาบันฝากเกี่น/ประเทศ			
				7,		
•			และจะจัดอื่นคำขอรับสิทธิบัด	ร/อนุสิทธิบัตรนีที่จัดทำ		
เป็นภาษาไทยภายใน 90 วัน นัก						
🔲 อังกฤษ 🔲 ฝรั่งเศส 🔲 เยอรมัน 🔲 ญี่ปุ่น 🔲 อื่นๆ 12.ผู้ขอรับสิทธิบัตร/อนุสิทธิบัตร ขอให้อธิบดีประกาศโพษณาคำขอรับสิทธิบัตร หรือรับจดทะเบียน และประกาศโพษณาอนุสิทธิบัตรนี้						
12.ผู้ของบลทรบคร/อนุลทรบะ หลังจากวันที่	เด็ดน เด็ดน		inauusingn nushisulu idi	งตาอนุสทธบดรน		
***************************************		ท.ศ ในการประเ	กาสโคเนคเว	·		
 ผู้ขอรับสิทธิบัตร/อนุสิทธิบัตรขอให้ไร้รูปเขียนหมายเลข ในการประกาศโจษณา 13.คำขอรับสิทธิบัตร/อนุสิทธิบัตรนี้ประกอบด้วย 14.เอกสารประกอบด้างอ 						
ก. แบกพิมพ์คำขอ 2 หน้า			☑ เอกสารแสดงสิทธิในการขอรับสิทธิบัตร/อนุสิทธิบัตร			
			□ หนังสือรับรองการแสดงการประดิษฐ์/การออกแบบ			
_	หรือทำพรรณนาแบบผลิตภัณฑ์ 6 หน้า ผลิตภัณฑ์					
ค. ข้อถือสิทษี 2	หน้า	่ ชานังส์	☑ หนังสือมอบอำนาจ			
ง, รูปเขียน รูป	หน้า	□ reut.	🔲 เอกสารราชละเอียดเกี่ยวกับจุลจีพ			
 ภาพแสดงแบบผลิตภัณฑ์ 	 ภาพแสดงแบบผลิตภัณฑ์ เอกสารการขอนับวันอื่นคำขอในค่างประเทศเป็น 		Jระเท สเป็นวันอื่น			
🗖 รัฦเลูณา รัว	ป หน้า	ค้าขอ	คำขอในประเทศไทย			
🗆 ภาพถ้าย 📑	ป หน้า	□ iana	🗖 เอกสารขอเปลี่ยนแปลงประเภทของสิทธิ			
ฉ. บทสรุปการประดิษฐ์	เ หน้า	🖂 เอบสา	🗹 เอกสารอื่น ๆ			
15. จ้าหเจ้าขอรับรองว่า						
 การประดิษฐ์นี้ไม่เคยอื่นขอรับสิทธิบัตร/อนุสิทธิบัตรมาก่อน 						
🗖 การประดิษฐ์นี้ได้พัฒนาปรับปรุงมาจาก						
16.ถายมือชื่อ (🔲 ผู้ขอรับสิทธิบัตร /อนุสิทธิบัตร; 🗹 ด้วแทน)						
עומטאפם וומשאר אס אר אין אין אין						

<u>หมายเทพ</u> บุคคลใดอื่นขอวับสิทธิบัตรการประดิษฐ์หรือการออกแบบหอิตภัณฑ์ หรืออนุสิทธิบัตร โดยการแฮพงร้อความอันเป็นเท็จแก่พนักงานเข้าหน้าที่ เพื่อให้ ได้ไปซึ่งสิทธิบัตรหรืออนุสิทธิบัตร ต้องระวางไทมชำลุกไม่เกินทกเดือน หรือปรับไม่เกินทำทันบาท หรือทั้งปรับ

แบบ สป/สม/อสป/ก01-ก หนัว 3 ของร้านวน 3 หนัว

3.ผู้ขอรับสิทธิบัคร/อนุสิทธิบัคร และที่อยู่ (เลขที่ ถนน บ่าะเทศ) จูทาลงกรณ์มหาวิทยาลัย อยู่ที่ จุฬาลงกรณ์มหาวิทยาลัย ถนนพญาไห แขวงวังใหม่ เขตปัจมวัน กรุงเทพฯ 10330 3.1 สัญหาติ ไทย 3.2 โทรศัพท์ 0-2218-2895-6 3.3 โทรสาร 0-2215-0115 สำนักงานกองทุนสนับสนุนการวิจัฮ อยู่ที่ ขั้น 14 อาการ เอส เอ็ม ทาวเวอร์ 979/17-21 ถนนพหลโตริน แขวงสามเสนใน เขคพญาไท กรุงเทพฯ 10400 3.1 ลัญชาติ ใหย 3.2 โทรศัพท์ 0-2298-0455 3.3 โทรสาร 0-2298-0476

หน้าที่ 1 ของจำนวน 6 หน้า

รายละเชียดการประดิษฐ์

ชื่อที่แสดงถึงการประดิษฐ์

5

10

15

20

25

30

เยื่อแผ่นสำหรับย่อยสลายสารพิษและเชื้อโรคด้วยแสง

ลักษณะและความมุ่งหมายของการประติษฐ์

การประดิษฐ์นี้เกี่ยวข้องกับเยื่อแผ่นลำหรับกระบวนการย่อยสลายสารพิษและเชื้อโรคด้วย แสง (Polymeric Membra.ies for Photocatalytic Degradation) ซึ่งประกอบด้วย โพลีอะคลิโลใน ไตรล์, ไดเมธิลฟอร์มามายด์ และ ไททาเนียมไดออกไซด์

ในอีกรูปแบบหนึ่งของการประดิษฐ์ เยื่อแผ่น ซึ่งประกอบด้วย โพลีไวนิลอะซิเตด, เตตระ ไฮโดรฟูแรน และ ไททาเนียมไดออกไซด์

ในอีกรูปแบบหนึ่งของการประดิษฐ์ เยื่อแผ่น ซึ่งประกอบด้วย เซลลูโลสอะซิเตด, อะซีโตน และ ไททาเบียมไดออกไซด์

ความมุ่งหมายของการประดิษฐ์นี้ เพื่อนำไปใช้สลายสารอินทรีย์จำพวกเบนซีนและอนุ พันธ์ของเบนซีน ซึ่งเป็นสารก่อโรคมะเร็งภายในร่างกายมนุษย์ และยังใช้ย่อยสลายเชื้อโรคและ แบคทีเรีย เยื่อเลือกผ่านนี้มีส่วนผสมของสารไททาเนียมไดออกไซด์ที่มีพื้นที่ผิวสูงสำหรับ กระบวนการสลายสารอินทรีย์ด้วยแสง

สาขาวิทยาการที่เกี่ยวข้องกับการประดิษฐ์

การประดิษฐ์นี้เกี่ยวร้องกับวิทยาการต่างๆ ได้แก่ การกำจัดน้ำเสียจากอุตสาหกรรมปิโตร เคมี โดยใช้กระบวนการแตกสลายสารอินทรีย์ด้วยแสง (Photocatalysis) กระบวนการเพิ่ม ไฮโดรเจนอะตอมแก้โมเลกุลของสารโพรไพร์ (Hydrogenation of propyne) กระบวนการเพิ่ม ออกซีเจนอะตอมแก่สารอินทรีย์ (Oxidation of organic compound) กระบวนการแยกแก็ส (Gas separation) และกระบวนการกำจัดแบคทีเรียด้วยแสง (Bactericidol activity of photocatalyst)

ภูมิหลังของศิลปะหรือวิทยาการที่เกี่ยวข้อง

กระบวนการย่อยสลายสารอินทรีย์และสารอนินทรีย์ที่เป็นองค์ประกอบในน้ำทิ้งจากโรง งานอุตสาหกรรมจัดว่าเป็นประเด็นสำคัญมากในปัจจุบัน ดังนั้น จึงได้รับความสนใจจาก นักวิทยาศาสตร์มากมายในการศึกษาและวิจัย เพื่อจุดมุ่งหมายในการเพิ่มประสิทธิภาพของการ กำจัดน้ำเสีย รวมถึงการกำจัดน้ำเสียด้วยกระบวนการที่ใช้ต้นทุนต่ำ และย่อยสลายสารโดยไม่ เหลือสารพิษตกค้างในน้ำ นอกจากนี้ ในปัจจุบันมลภาวะจากสิ่งแวดล้อมเป็นปัญหาที่ต้องแก้ไข

หน้าที่ 2 ของจำนวน 6 หน้า

โดยเร็ว ซึ่งมลภาวะเหล่านี้ ได้แก่ อนุภาคสิ่งมีชีวิตขนาดเล็กที่พบในน้ำ และอากาศ การกำจัดเชื้อ โรคต่างๆ ในน้ำนั้นมีประโยชน์โดยตรงต่อการอุปโกค บริโภคของมนุษย์ อีกทั้งยังมีผลต่อการผลิต ผลิตภัณฑ์ต่างๆ ที่ใช้ในคน และสัตว์ กระบวนการการกำจัดเชื้อโรคในอากาศนั้นมีความสำคัญ มากในทางการแพทย์ ซึ่งต้องการความระมัดระวังเป็นอย่างสูงในเรื่องการปนเปื้อนของสารทาง ชีวภาพต่างๆ เนื่องจากในกระบวนการทดลองเกี่ยวกับสัตว์ พืช และคนนั้นมีโอกาสที่จะติดเชื้อได้ ง่าย กระบวนการกำจัดที่ใช้กันอย่างแพร่หลายในประเทศพัฒนาแล้วคือ วิธีการเพิ่มคลอรีน (Chlorination) การเติมโอโซน (Ozonation) และกระบวนการย่อยสลายด้วยแสง (Photocatalytic degradation) ซึ่งเป็นวิธีที่มีประสิทธิภาพและใช้ในระดับใหญ่

กระบวนการย่อยสลายสารด้วยแลงเป็นกระบวนการที่มีประสิทธิภาพสูงซึ่งใช้พลังงานแลง จากธรรมชาติและแลงที่ประสิษฐ์ชื่นเป็นแหล่งพลังงานที่ใช้ในกระบวนการย่อยสลายสารโดยใช้ สารไททาเนียมไดออกไซด์เป็นตัวเร่งปฏิกิริยา ซึ่งสารไททาเนียมไดออกไซด์นี้มีประสิทธิภาพสูงและ ใช้กันอย่างแพร่หลาย นอกจากนั้น ยังมีความเสถียรต่อสารเคมีสูง และที่ลำคัญมากกว่านั้น คือ เป็นสารที่ไม่เป็นพิษต่อสิ่งแวดล้อมอีกด้วย ในปัจจุบันกระบวนการย่อยสลายด้วยแสงที่มีสารไททา เนียมไดออกไซด์เป็นองค์ประกอบนั้นเป็นที่ยอมรับและใช้กันอย่างแพร่หลายรวมทั้งมีการศึกษา วิจัยและพัฒนาเพื่อใช้กับการใช้งานในรูปแบบใหม่ๆ เช่น หน้ากากกำจัดแบคทีเรีย (Environmental safety mask and respirator) ระบบกรองอากาศด้วยกระบวนการย่อยสลายสาร ด้วยแสง (Photocatalytic air filtration system) ระบบการกำจัดเชื้อรา จุลินทรีย์ เชื้อใจรัส และ แบคทีเรียในน้ำ (Deactivation of fungi, microorganisms, viruses and bacteria in water) นอกจากนี้ยังมีการใช้ปฏิกิริยาการย่อยสลายด้วยแสงที่มีสารไททาเนียมไดออกไซด์เป็นองค์ประ กอบในการสลายเซลล์มะเร็ง และเนื้องอก อีกทั้งยังใช้ในทางทันตกรรม คือ เป็นวัสดุจุดพัน เพื่อ ป้องกันการเจริญเติบโตของแบคทีเรียในช่องปาก และใช้เป็นองค์ประกอบในแปรงสีพันที่มีการ กระตุ้นด้วยแสง (Light activated tooth brush)

10

15

20

25

30

ข้อเสียของกระบวนการย่อยสลายสารด้วยแสงในน้ำเกิดขึ้น เนื่องจากต้องใช้กระบวนการ แยกของเหลวออกจากของแข็งที่เกิดจากการกระจายตัวของสารไททาเนียมไดออกไรด์ในน้ำ หลังจากเสร็จสิ้นกระบวนการย่อยสลายซึ่งกระบวนการนี้มีราคาแพง และใช้เวลานาน ในปัจจุบัน ได้มีการแก้ไขข้อเสียดังกล่าวโดยการใช้เยื่อแผ่นที่มีสารไททาเนียมไดออกไรด์กระจายตัวผังอยู่ใน เยื่อแผ่น ดังนั้น เยื่อแผ่นที่ประกอบด้วยสารไททาเนียมไดออกไขด์จึงเป็นที่สนใจและใช้กันอย่าง แพร่หลายเนื่องจากเยื่อแผ่นนี้มีลักษณะเฉพาะคือ มีปริมาณการไหลผ่านของน้ำสูง มีคุณสมบัติใน การเป็นสารกึ่งตัวนำ มีประสิทธิภาพในการย่อยสลายสารอินทรีย์ และมีความเสถียรต่อสารเคมีสูง อีกทั้งยังลดกระบวนการในการแยกสารไททาเนียมไดออกไรด์ออกจากสารผสมอีกด้วย